by adding 2× SDS sample buffer, separated by SDS-PAGE, and subjected to immunoblotting with polyclonal anti-RUNX3 antibody.

In Vitro Pulldown Assay—Wild-type p53 and its deletion mutants were generated *in vitro* using a T7 Quick-coupled transcription/translation system (Promega, Madison, WI) in the presence of [^{35}S]methionine according to the manufacturer's recommendations. Cell lysates prepared from COS7 cells transfected with the expression plasmid encoding RUNX3 were mixed and incubated overnight at 4 °C. Reaction mixtures were then immunoprecipitated with anti-RUNX3 antibody. The immunoprecipitates were washed extensively with the lysis buffer and resolved by SDS-PAGE. The gels were dried up and subjected to autoradiography.

Indirect Immunofluorescence Staining—U2OS cells were grown on coverslips and transiently transfected with the expression plasmid for RUNX3. Twenty four hours after transfection, cells were treated with 0.5 μM of ADR or left untreated. Forty eight hours after ADR treatment, cells were fixed in 3.7% formaldehyde in PBS for 30 min at room temperature, permeabilized in 0.2% Triton X-100 in PBS for 5 min at room temperature, and blocked with 3% bovine serum albumin in PBS for 1 h at room temperature. After blocking, cells were then simultaneously incubated with polyclonal anti-RUNX3 and monoclonal anti-p53 antibodies followed by incubation with fluorescein isothiocyanate-conjugated goat anti-rabbit IgG and rhodamine-conjugated goat anti-mouse IgG. Cell nuclei were stained with DAPI (Vector Laboratories, Burlingame, CA). Cells were imaged by Fluoview laser scanning confocal microscope (Olympus, Tokyo, Japan).

Subcellular Fractionation—U2OS cells were transiently transfected with the expression plasmid encoding RUNX3. Twenty eight hours after transfection, cells were treated with 0.5 μM ADR or left untreated. Forty eight hours after ADR treatment, cells were washed in ice-cold PBS and lysed in lysis buffer containing 10 mM Tris-HCl, pH 8.0, 1 mM EDTA, 0.5% Nonidet P-40, and protease inhibitor mixture for 30 min at 4 °C. Reaction mixture was centrifuged at 15,000 rpm at 4 °C to separate the soluble fraction (cytoplasmic fraction) from the insoluble fraction (nuclear fraction). Equal amounts of cytoplasmic and nuclear fractions were separated by SDS-PAGE and immunoblotted with anti-RUNX3 antibody. Each fraction was analyzed by immunoblotting with monoclonal anti-lamin B (Ab-1, Oncogene Research Products) or with monoclonal anti-α-tubulin antibody (Ab-2, NeoMarkers, Fremont, CA) to show the purity of each fraction.

Apoptotic Assay—U2OS and H1299 cells were transiently co-transfected with the constant amount of the expression plasmid for GFP together with or without the increasing amounts of RUNX3 expression plasmid. Forty eight hours after transfection, cells were fixed in 3.7% formaldehyde in PBS for 30 min at room temperature and permeabilized in 0.2% Triton X-100 in PBS for 5 min at room temperature. The coverslips were mounted with DAPI-containing mounting medium (Vector Laboratories) and observed under a Fluoview laser scanning confocal microscope (Olympus, Tokyo, Japan). The number of GFP-positive cells with apoptotic nuclei was measured.

FACS Analysis—H1299, HeLa, U2OS, and SAOS-2 cells were transiently transfected with control siRNA or with siRNA against RUNX3. Twenty four hours after transfection, cells were exposed to the indicated concentrations of ADR. Forty eight hours after ADR treatment, floating and attached cells were collected, washed in PBS, and fixed in 70% ethanol at −20 °C. Following incubation in PBS containing 40 μg/ml propidium iodide and 200 μg/ml of RNase A for 1 h at room temperature in the dark, stained nuclei were analyzed on a FACScan machine (BD Biosciences).

Luciferase Reporter Assay—H1299 cells were plated in a 12-well flat bottom plates on a day prior to transfection at a density of 50,000 cells/well. Cells were then co-transfected with 12.5 ng of p53 expression plasmid, 100 ng of p53-responsible luciferase reporter construct ($p21^{WAF1}$ or BAX), and 10 ng of pRL-TK *Renilla* luciferase cDNA together with or without the increasing amounts of the RUNX3 expression plasmid (100 and 300 ng). Total amount of plasmid DNA per transfection was kept constant (510 ng) with an empty plasmid pcDNA3 (Invitrogen). Forty eight hours after transfection, cells were lysed, and both firefly and *Renilla* luciferase activities were measured with Dual-Luciferase reporter assay system (Promega), according to the manufacturer's instructions. The firefly luminescence signal was normalized based on the *Renilla* luminescence signal.

Small Interfering RNA—U2OS cells were transiently transfected with a SMART pool siRNA specifically designed against RUNX3 or a control nontargeting siRNA (Dharmacon, Chicago) by using Lipofectamine RNAiMAX transfection reagent (Invitrogen) according to the manufacturer's instructions. Forty eight hours after transfection, total RNA was prepared and subjected to RT-PCR. For knocking down of the endogenous p53, U2OS cells were transiently transfected with the empty plasmid (pSUPER, OligoEngine, Seattle, WA) or with pSUPER expression plasmid encoding siRNA against p53 (pSUPER-siRNA-p53) by using Lipofectamine 2000 transfection reagent (Invitrogen) according to the manufacturer's instruction.

Colony Formation Assay—H1299 cells were seeded at a final density of 200,000 cells/6-well plate and allowed to attach overnight. Cells were then co-transfected with the indicated combinations of the expression plasmids. Total amount of plasmid DNA per transfection was kept constant (2 μg) with pcDNA3. Forty eight hours after transfection, cells were transferred to the fresh medium containing G418 (800 μg/ml). After 14 days, viable colonies were washed in PBS and stained with Giemsa solution.

RESULTS

siRNA-mediated Knockdown of RUNX3 Decreases the Drug Sensitivity in a p53-dependent Manner—To address whether RUNX3 could be involved in p53-mediated DNA damage response, *RUNX3* was knocked down in human osteosarcoma-derived U2OS, human lung carcinoma-derived A549, human lung carcinoma-derived H1299, human cervical carcinoma-derived HeLa, and human osteosarcoma-derived SAOS-2 cells (Fig. 1*A*). U2OS and A549 cells carry wild-type *p53*. On the other hand, H1299 and SAOS-2 cells are *p53*-null and HeLa

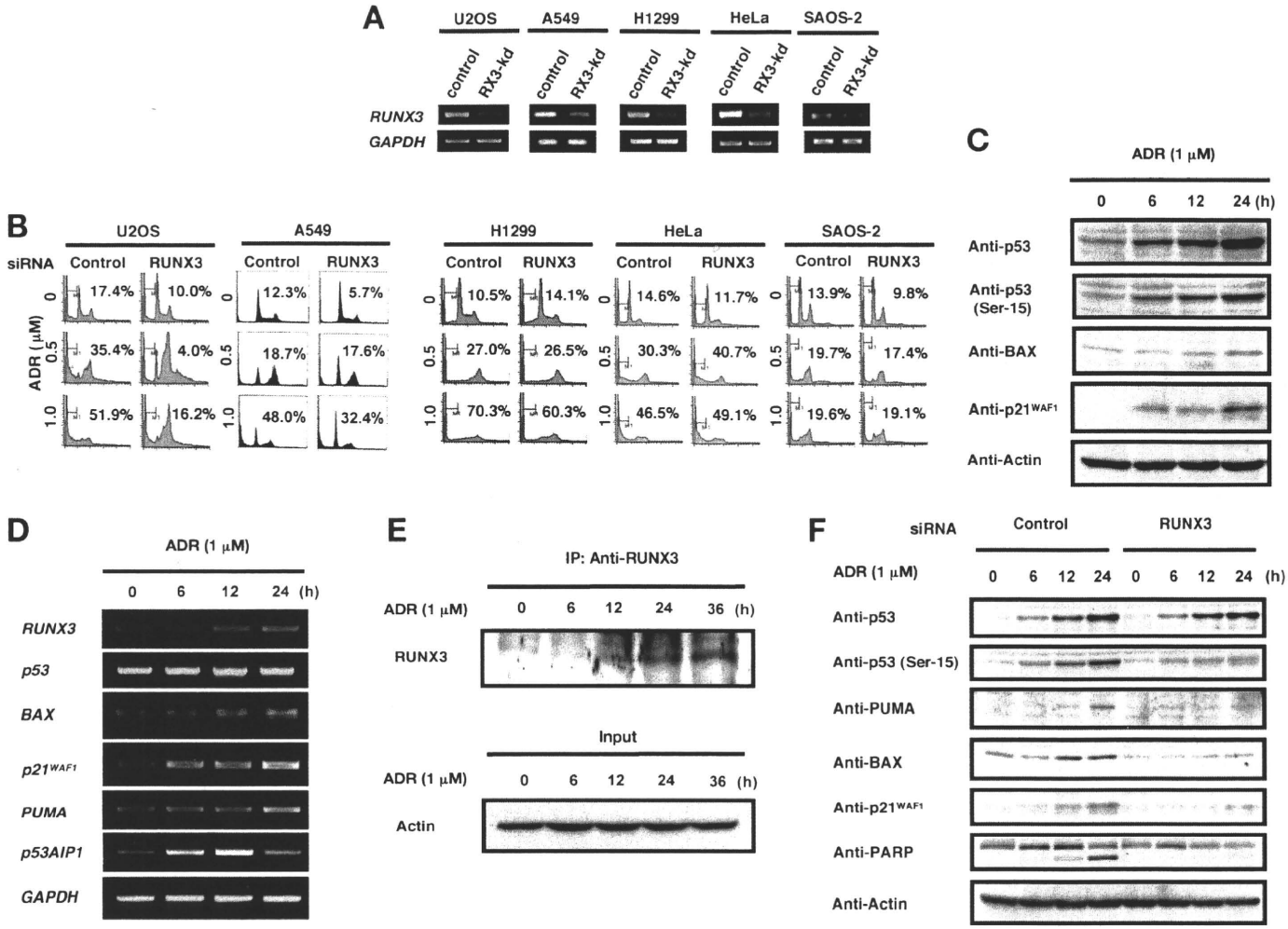

FIGURE 1. **Silencing of RUNX3 inhibits ADR-dependent apoptotic cell death in *p53*-proficient cells but not in *p53*-deficient cells.** *A*, siRNA-mediated knockdown of the endogenous RUNX3. The indicated cell lines were transiently transfected with control siRNA (*control*) or with siRNA against RUNX3 (*RX3-kd*). Forty eight hours after transfection, total RNA was prepared and subjected to RT-PCR. *B*, FACS analysis. Transfected cells were treated with the indicated concentrations of ADR or left untreated. Forty eight hours after ADR treatment, floating and attached cells were collected, and the percentage of cells with sub-G_1 DNA content was analyzed by FACS. *C–E*, ADR-mediated induction of RUNX3. U2OS cells were exposed to ADR at a final concentration of 1 μM. At the indicated times after ADR treatment, cell lysates and total RNA were prepared and processed for immunoblotting (*IB*) (*C*) and RT-PCR (*D*), respectively. Actin and *GAPDH* were used as loading and internal controls, respectively. For the detection of RUNX3, cell lysates were immunoprecipitated (*IP*) with anti-RUNX3 antibody followed by immunoblotting with anti-RUNX3 antibody (*E*). *F*, RUNX3 affects the phosphorylation status of p53 in response to ADR. U2OS cells were transiently transfected with control siRNA or with siRNA targeting RUNX3 and treated with ADR (at a final concentration of 1 μM). At the indicated time points after ADR treatment, cell lysates were prepared and subjected to immunoblotting with the indicated antibodies. Actin was used as a loading control.

cells lack functional p53 due to the presence of viral E6 protein (27, 28). Knocked down cells were then exposed to the indicated concentrations of DNA-damaging reagent, adriamycin (ADR). As shown in Fig. 1*B*, silencing of *RUNX3* had undetectable effects on ADR-induced apoptotic cell death in H1299, HeLa, and SAOS-2 cells, whereas ADR-mediated apoptotic cell death was significantly inhibited in U2OS and A549 cells. Similar results were also obtained in cells treated with other DNA-damaging drugs, including etoposide and camptothecin, but not with paclitaxel (supplemental Fig. S1). These results suggest a presence of functional association between RUNX3 and p53 in response to DNA damage.

We next examined whether RUNX3 could be induced in response to DNA damage. U2OS cells treated with ADR at a final concentration of 1 μM induced the accumulation of p53 and its phosphorylation at Ser-15 as well as expression of its target genes such as *BAX*, *p21*^{WAF1}, *PUMA*, and *p53AIP1* (Fig. 1, *C* and *D*). Under our experimental conditions, *RUNX3* was significantly up-regulated at both mRNA (Fig. 1*D*) and protein (Fig. 1*E*) levels. These observations indicate that *RUNX3* is one of the DNA damage-response genes. In addition, we could not detect ADR-mediated phosphorylation of p53 at Ser-20 and Ser-46 under our experimental conditions (data not shown).

These results prompted us to examine the functional relationship between RUNX3 and p53 in response to DNA damage. To this end, U2OS cells were transiently transfected with the control siRNA or with siRNA against RUNX3 and then exposed to ADR. As shown in Fig. 1*F*, the knocking down of *RUNX3* had a negligible effect on ADR-dependent accumulation of p53, whereas ADR-dependent phosphorylation of p53 at Ser-15 was markedly abrogated. Consistent with these results, ADR-mediated induction of p53 target gene products was strongly inhibited in *RUNX3*-knocked down cells. Additionally, ADR-dependent cleavage of PARP was undetectable in *RUNX3*-knocked down cells. Thus, our present findings imply that RUNX3 contributes to the regulation of DNA damage-induced phosphory-

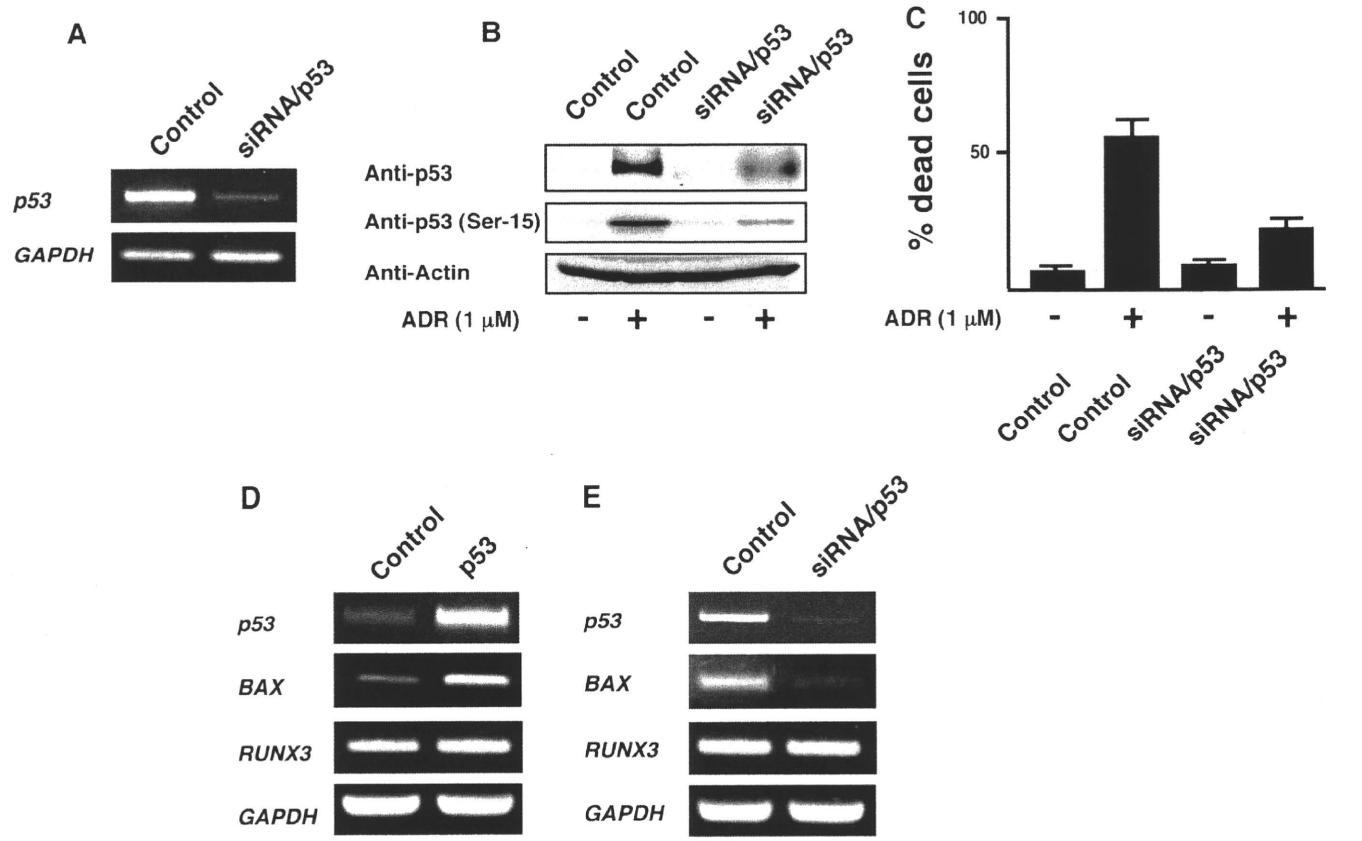

FIGURE 2. **U2OS cells undergo apoptotic cell death in a p53-dependent manner.** *A*, siRNA-mediated knockdown of the endogenous *p53*. U2OS cells were transiently transfected with the empty plasmid (pSUPER) or with the expression plasmid for siRNA against p53 (pSUPER-siRNA-p53). Forty eight hours after transfection, total RNA was prepared and subjected to RT-PCR. *GAPDH* was used as an internal control. *B*, siRNA-mediated knockdown of p53 reduces its accumulation and phosphorylation in response to ADR. U2OS cells were transiently transfected with the empty plasmid or with the expression plasmid for siRNA targeting p53. Twenty four hours after transfection, cells were treated with 1 μM ADR or left untreated. Forty eight hours after ADR treatment, whole cell lysates were prepared and processed for immunoblotting with anti-p53 antibody or with antibody against phospho-p53 at Ser-15. Actin was used as a loading control. *C*, trypan blue exclusion assay. U2OS cells were transiently transfected as in *B*. Forty eight hours after ADR treatment, floating and attached cells were collected and stained with 0.4% trypan blue. After trypan blue staining, a number of trypan blue-positive cells were measured. *D* and *E*, *RUNX3* is not a direct transcriptional target of p53. U2OS cells were transiently transfected with the empty plasmid or with the expression plasmid for p53. Forty eight hours after transfection, total RNA was prepared and subjected to RT-PCR. *BAX* and *GAPDH* were used as a positive and an internal control, respectively (*D*). Similarly, U2OS cells were transiently transfected with the empty plasmid or with the expression plasmid for siRNA against p53. Forty eight hours after transfection, total RNA was prepared and processed for RT-PCR. *BAX* and *GAPDH* were used as a positive and an internal control, respectively (*E*).

lation of p53 at Ser-15 and thereby acting as a co-activator for p53 with undetectable effect on its stability. This may give some clues to understand the previous observations as described by Ashcroft *et al.* (29) showing that DNA damage-induced stabilization of p53 is detectable irrespective of its phosphorylation status, although both phenomena usually occur in parallel (20).

RUNX3 Is Not a Direct Transcriptional Target of p53—Consistent with the previous observations (30), our present results strongly suggest that U2OS cells undergo apoptotic cell death in a p53-dependent manner. To further confirm this issue, we have performed siRNA-mediated knockdown of the endogenous *p53* in U2OS cells. U2OS cells were transiently transfected with the empty plasmid or with the expression plasmid for siRNA against p53. Forty eight hours after transfection, total RNA was prepared and subjected to RT-PCR. As clearly shown in Fig. 2*A*, the amounts of the endogenous *p53* significantly reduced in the presence of siRNA against p53 under our experimental conditions. Next, the knocked down cells were treated with ADR or left untreated. Forty eight hours after ADR treatment, whole cell lysates were prepared and analyzed by immunoblotting. As shown in Fig. 2*B*, siRNA-mediated knocking down of the endogenous *p53* resulted in a remarkable inhibition of ADR-dependent accumulation of p53 as well as ADR-dependent phosphorylation of p53 at Ser-15. In accordance with these results, knocking down of the endogenous *p53* led to a significant reduction in number of dead cells in the presence of ADR as compared with the control cells exposed to ADR (Fig. 2*C*). Intriguingly, a substantial number of dead cells was detectable in ADR-treated knockdown cells, which might be due to the pro-apoptotic effect of the remaining p53 and/or the other p53 family members such as p73 (31). Taken together, U2OS cells underwent apoptotic cell death at least in part in a p53-dependent manner.

Because there existed a clear correlation between ADR-dependent phosphorylation of p53 at Ser-15 and transcriptional induction of *RUNX3*, it is likely that *RUNX3* could be one of the direct target genes of p53. To address this issue, U2OS cells were transiently transfected with the empty plasmid or with the expression plasmid for p53. As shown in Fig. 2*D*, forced expression of p53 resulted in a significant induction of *BAX*, whereas the expression levels of the endogenous *RUNX3* remained

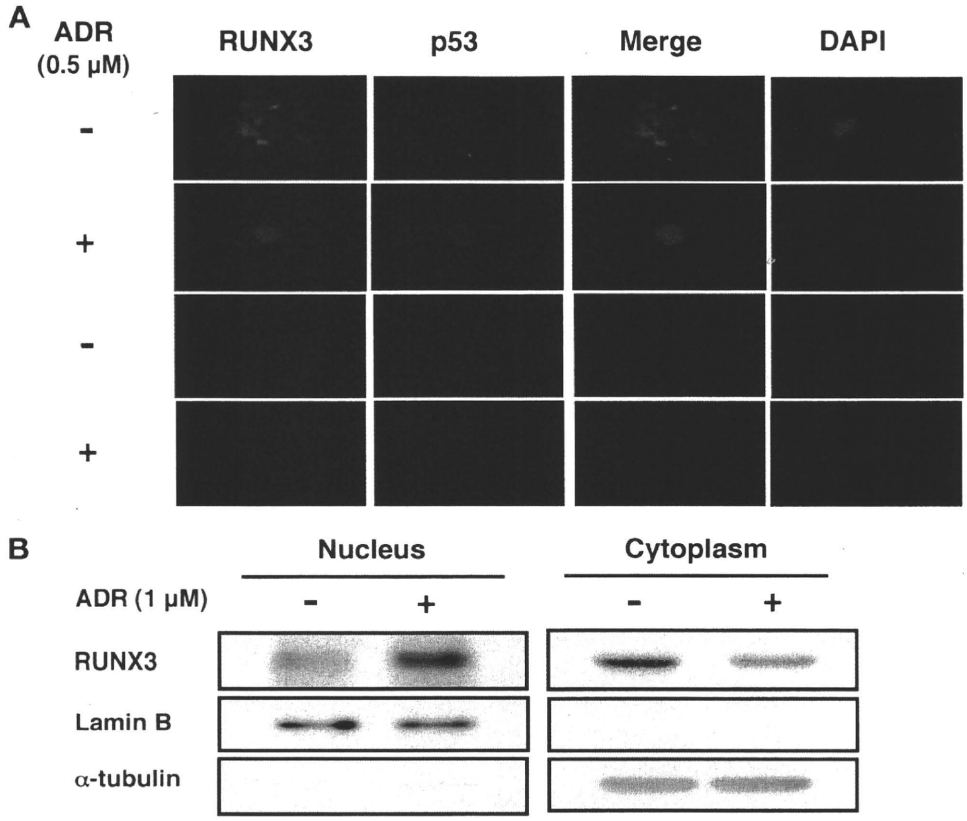

FIGURE 3. **ADR-mediated nuclear translocation of RUNX3.** *A*, indirect immunofluorescent staining. U2OS cells were transiently transfected with the expression plasmid for RUNX3. Twenty four hours after transfection, cells were treated with ADR or left untreated. Forty eight hours after ADR treatment, cells were simultaneously stained with anti-RUNX3 and anti-p53 antibodies. Cell nuclei were stained with DAPI. *Lower panels* show negative control experiments without primary antibodies. Merged images indicate nuclear co-localization of RUNX3 with p53 in the presence of ADR. *B*, immunoblotting. U2OS cells were transiently transfected as in *A*. Twenty four hours after transfection, cells were treated with ADR or left untreated. Forty eight hours after ADR treatment, cells were biochemically fractionated into nuclear and cytoplasmic fractions. Each fraction was subjected to immunoblotting with anti-RUNX3 antibody (*top panel*). Samples were immunoblotted with anti-lamin B (*middle panel*) or with anti-α-tubulin antibody (*bottom panel*) to show the purity of each fraction.

unchanged even in the presence of the exogenously expressed p53. To further confirm these results, we performed siRNA-mediated knockdown of the endogenous *p53*. As seen in Fig. 2*E*, a significant down-regulation of *BAX* was detectable in *p53*-knocked down cells, whereas siRNA-mediated knocking down of *p53* had an undetectable effect on the expression levels of the endogenous *RUNX3*. Thus, it is conceivable that *RUNX3* might not be a direct target gene of p53. Indeed, we failed to find out the putative p53-responsive element within the 5′-upstream region (~1 kb) of human *RUNX3* gene. At present, the precise molecular mechanisms behind ADR-mediated up-regulation of *RUNX3* remained to be elusive.

Interaction between RUNX3 and p53 in Cells—It has been shown that nuclear translocation of RUNX3 plays a critical role in the regulation of apoptotic cell death (16, 17). Our indirect immunofluorescence staining and biochemical fractionation experiments revealed that RUNX3 is induced to translocate from the cytoplasm into the cell nucleus in response to ADR and co-localizes with p53 (Fig. 3, *A* and *B*), suggesting that RUNX3 might form a complex with p53 in cells.

To further confirm this issue, we performed co-immunoprecipitation analysis using cell lysates prepared from U2OS cells exposed to ADR. As shown in Fig. 4*A*, the endogenous RUNX3 was co-immunoprecipitated with stress-induced p53 in U2OS cells. In accordance with these results, the anti-RUNX3 immunoprecipitates contained the endogenous p53. Similar results were also obtained in over-expression systems and *in vitro* pull-down assay (supplemental Fig. S2). Interestingly, RUNX3 was associated with another p53 family member p73 but not with p63 as examined by co-immunoprecipitation analysis (supplemental Fig. S3).

To identify essential region(s) of p53 required for interaction with RUNX3, we carried out *in vitro* pull-down assay using the indicated deletion mutants of p53 (Fig. 4*B*). Wild-type p53 and p53(102–393) were efficiently co-immunoprecipitated with RUNX3, whereas p53(1–353), p53(1–292), and p53(1–101) were not, suggesting that its extreme COOH-terminal region is required for the interaction with RUNX3. We also defined region(s) of RUNX3 essential for the interaction with p53 (Fig. 4*C*). Wild-type RUNX3 but not RUNX3(1–198) and RUNX3(1–67) was co-immunoprecipitated with p53, indicating that COOH-terminal region of RUNX3 is required for the complex formation with p53.

RUNX3 Acts as a Co-activator for p53—To further examine the functional significance of the interaction between RUNX3 and p53, we performed luciferase reporter assays. As shown in Fig. 5*A*, RUNX3 had an ability to enhance p53-mediated luciferase activities driven by $p21^{WAF1}$ and *BAX* promoters in a dose-dependent manner. In a good agreement with these observations, RUNX3 increased p53-dependent expression of the endogenous $p21^{WAF1}$, *PUMA*, and *BAX* as examined by RT-PCR (Fig. 5*B*), indicating that RUNX3 acts as a co-activator for p53. We then asked whether RUNX3 could affect p53-dependent apoptotic cell death. Co-expression of p53 with RUNX3 resulted in a remarkable reduction in number of drug-resistant colonies as compared with cells expressing p53 alone (Fig. 5*C*). Furthermore, a number of GFP-positive cells with apoptotic nuclei increased in U2OS cells expressing RUNX3 relative to control transfectants, whereas forced expression of RUNX3 increased the number of apoptotic cells to a significantly lesser degree in *p53*-deficient H1299 cells (Fig. 5*D*). Thus, it is likely that RUNX3 enhances both transcriptional and pro-apoptotic activities of p53.

Based on our present results, it is likely that the regulation of DNA damage-mediated phosphorylation of p53 at Ser-15

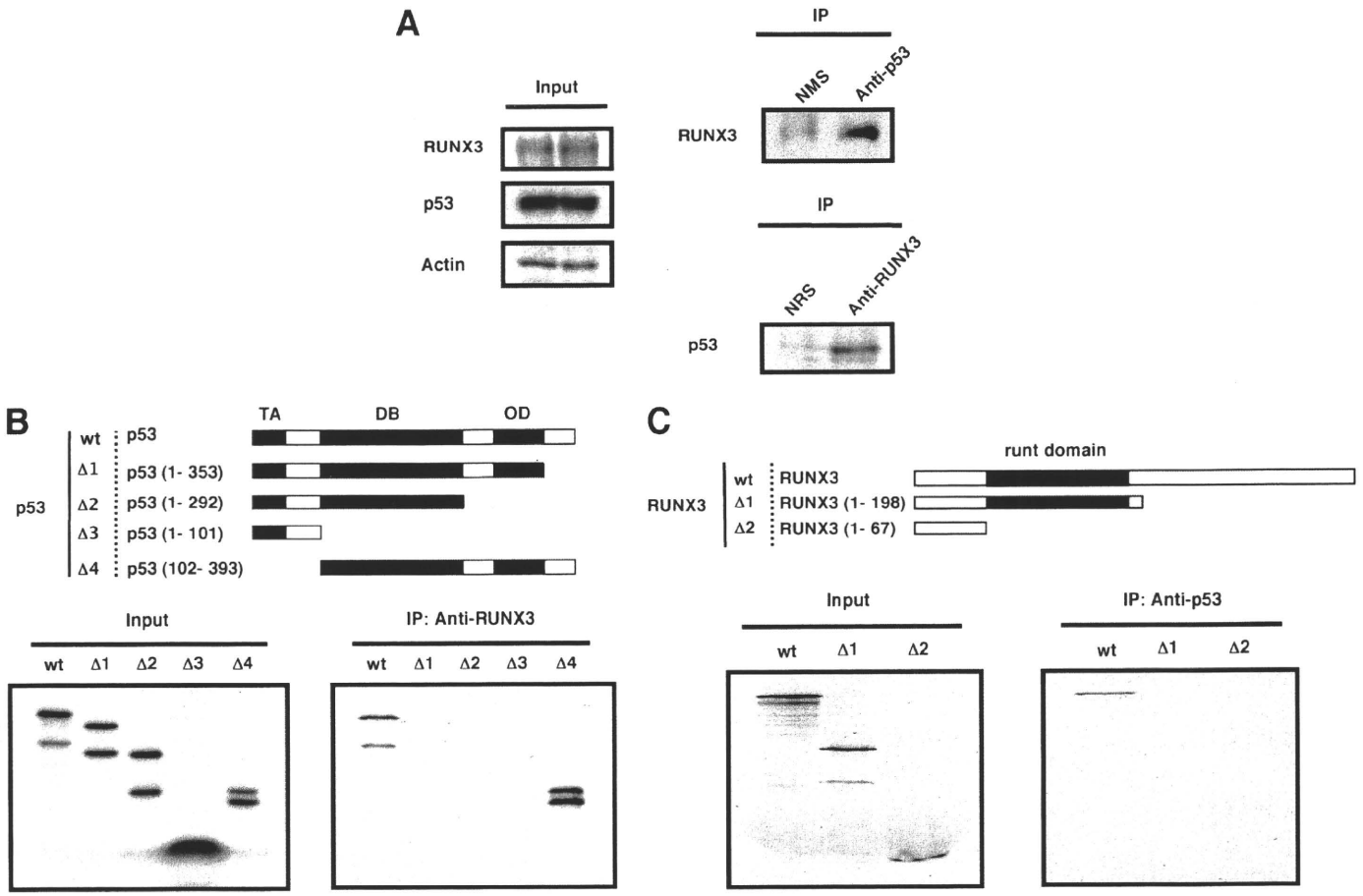

FIGURE 4. **Physical interaction between RUNX3 and p53 in cells.** *A*, endogenous interaction between RUNX3 and p53. Lysates prepared from ADR-treated U2OS cells were immunoprecipitated (*IP*) with mouse normal serum (*NMS*) or with anti-p53 antibody followed by immunoblotting with anti-RUNX3 antibody (*right panel*). 1/20 of inputs are shown in *left panel*. Reciprocal experiments are also shown in *right panel*. *B* and *C*, COOH-terminal regions of both proteins are required for their interactions. The indicated radiolabeled p53 derivatives were incubated with lysates prepared from COS7 cells expressing RUNX3 and immunoprecipitated with anti-RUNX3 antibody followed by autoradiography (*B*). The indicated radiolabeled RUNX3 derivatives were incubated with lysates prepared from COS7 cells and were subjected to immunoprecipitation with anti-p53 antibody followed by autoradiography (*C*). *wt*, wild type; *TA*, transactivation domain; *DB*, DNA-binding domain; *OD*, oligomerization domain.

is a major role of RUNX3. To gain molecular insights into understanding how RUNX3 could affect DNA damage-mediated phosphorylation of p53 at Ser-15, we examined whether ATM could have functional relevance to RUNX3. As shown in Fig. 6*A*, RUNX3 induced proteolytic cleavage of PARP and phosphorylation of p53 at Ser-15 in U2OS cells, indicating that RUNX3 might have an ability to promote phosphorylation of p53 at Ser-15, and thereby enhancing the transcriptional and pro-apoptotic activities of p53. Next, we have examined whether RUNX3 could interact with phosphorylated forms of ATM. To this end, HeLa cells were transiently transfected with the expression plasmid for RUNX3 and exposed to ADR. As shown in Fig. 6*B*, the anti-RUNX3 immunoprecipitates contained phosphorylated forms of ATM. These results imply that RUNX3 forms a complex with phosphorylated forms of ATM in response to ADR. To further investigate the functional relationship between RUNX3 and ATM, we employed wild-type and ATM-null A-T cells. As shown in Fig. 6*C*, the exogenous RUNX3 enhanced the phosphorylation of p53 at Ser-15, which was further augmented in wild-type cells but not in A-T cells exposed to ADR. Of note, the exogenous RUNX3 had an ability to enhance the ADR-mediated phosphorylation level of p53 at Ser-15. These results suggest that RUNX3 recruits phosphorylated forms of ATM onto p53 and thereby induces ATM-dependent phosphorylation of p53 at Ser-15 after DNA damage.

These findings prompted us to ask whether RUNX3 could affect the extent of ADR-mediated DNA damage. For this purpose, U2OS cells were transiently transfected with control siRNA or with siRNA against RUNX3 and exposed to ADR or left untreated. Twenty four hours after the treatment, total RNA and nuclear lysates were prepared and subjected to RT-PCR and immunoblotting, respectively. As shown in Fig. 7, ADR-mediated up-regulation of the endogenous *RUNX3* in cells transfected with control siRNA was detectable, and siRNA-mediated knocking down of the endogenous *RUNX3* was successful under our experimental conditions. Consistent with the previous observations (32), immunoblot analysis revealed that the expression levels of total ATM remain unchanged regardless of DNA damage. Of note, knocking down of the endogenous *RUNX3* had a marginal effect on the phosphorylation levels of ATM in response to ADR; however, we did not observe a significant difference of ADR-dependent accumulation of γH2AX (the phosphorylated form of histone H2AX) between control cells and *RUNX3*-knocked down cells,

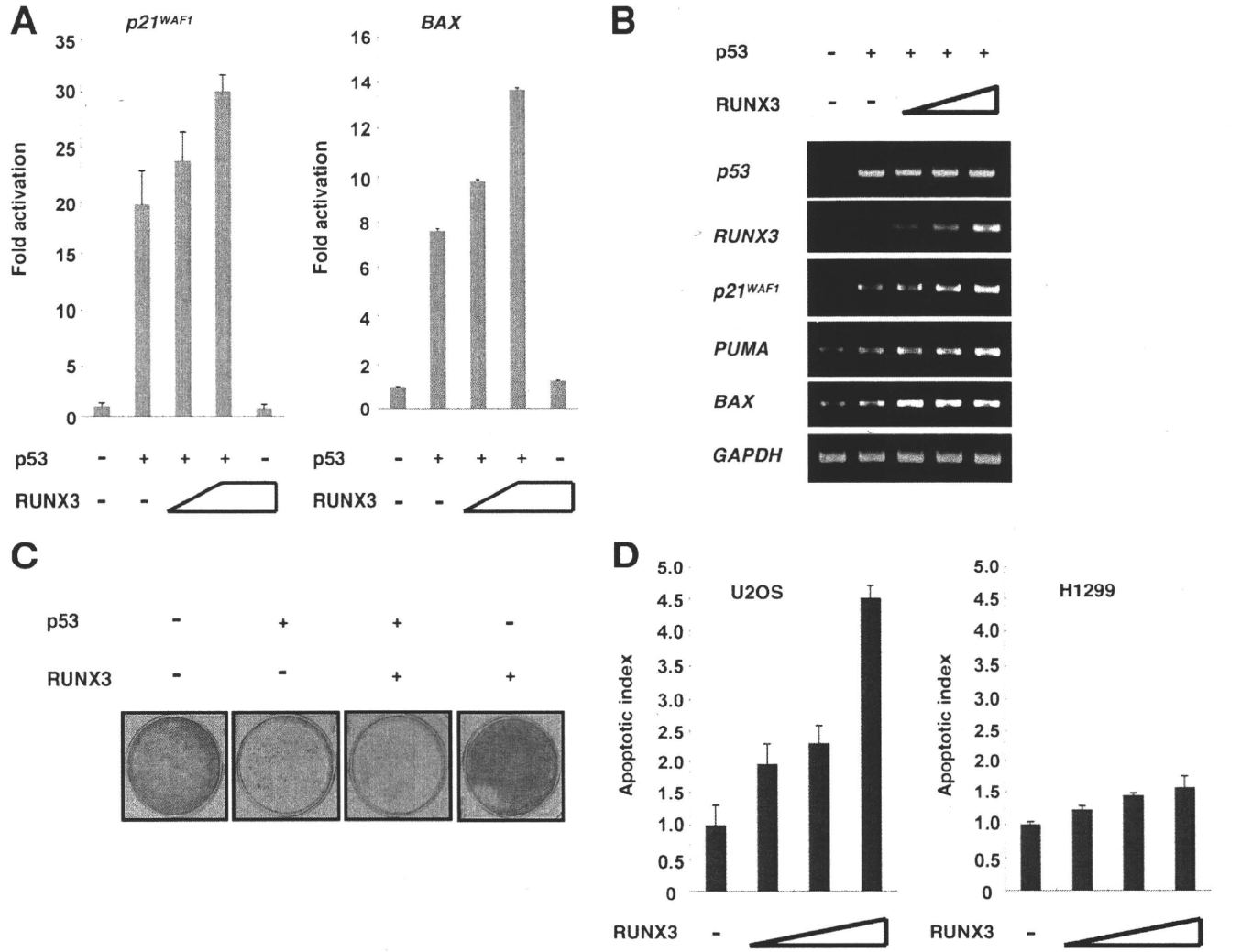

FIGURE 5. **RUNX3 acts as a co-activator for p53.** *A* and *B*, RUNX3 enhances p53-mediated transcriptional activation. *p53*-deficient human lung carcinoma-derived H1299 cells were transiently co-transfected with a constant amount of p53 expression plasmid, the luciferase reporter construct bearing p53-responsive element derived from human $p21^{WAF1}$ or *BAX* promoter and *Renilla* luciferase plasmid together with or without the increasing amounts of RUNX3 expression plasmid. Forty eight hours after transfection, cells were lysed, and their luciferase activities were measured *A*. H1299 cells were transiently transfected with the constant amount of the expression plasmid for p53 along with or without the increasing amounts of the expression plasmid encoding RUNX3. Forty eight hours after transfection, total RNA was prepared and processed for RT-PCR. *GAPDH* was used as an internal control. *C* and *D*, RUNX3 enhances pro-apoptotic activity of p53. H1299 cells were transfected with the indicated combinations of expression plasmids. Forty eight hours after transfection, cells were transferred into fresh medium containing G418 at a final concentration of 800 μg/ml. Two weeks after the selection with G418, drug-resistant colonies were stained with Giemsa solution (*C*). U2OS and H1299 cells were transiently transfected with a constant amount of GFP expression plasmid together with or without the increasing amounts of RUNX3 expression plasmid. Forty eight hours after transfection, a number of GFP-positive cells with apoptotic nuclei was measured (*D*).

suggesting that RUNX3 does not affect the extent of DNA damage.

Clinical Significance—We next examined whether *p53* inactivation and decreased expression of *RUNX3* could affect clinical prognosis of human cancer. For this purpose, we selected 105 patients with lung adenocarcinoma, in which *p53* mutations and its transcriptional silencing have been described (33). As shown in Fig. 8, long term cumulative survival rates were significantly decreased in the combination of *p53* mutation and low expression of *RUNX3* (p = 0.0203). Notably, the combined *p53* mutation and decreased expression of *RUNX3* were found in 25 patients in stages II to IV cancer (93%) compared with only 2 in stage I cancer (7%) (Fig. 7, p = 0.0018). These results suggest that functional interaction between RUNX3 and p53 might be associated with the clinical outcome of patients with lung adenocarcinoma.

DISCUSSION

To our knowledge, it remained unclear whether and how RUNX3 could be involved in the regulation of DNA damage response. In this study, we have found for the first time that RUNX3 modulates DNA damage-induced phosphorylation of tumor suppressor p53 at Ser-15 and thereby acting as a co-activator for p53. Thus, our present findings provide a novel insight into understanding the molecular mechanisms behind p53-dependent apoptotic cell death in response to DNA damage.

Under our experimental conditions, siRNA-mediated silencing of the endogenous *RUNX3* strongly inhibited apoptotic cell

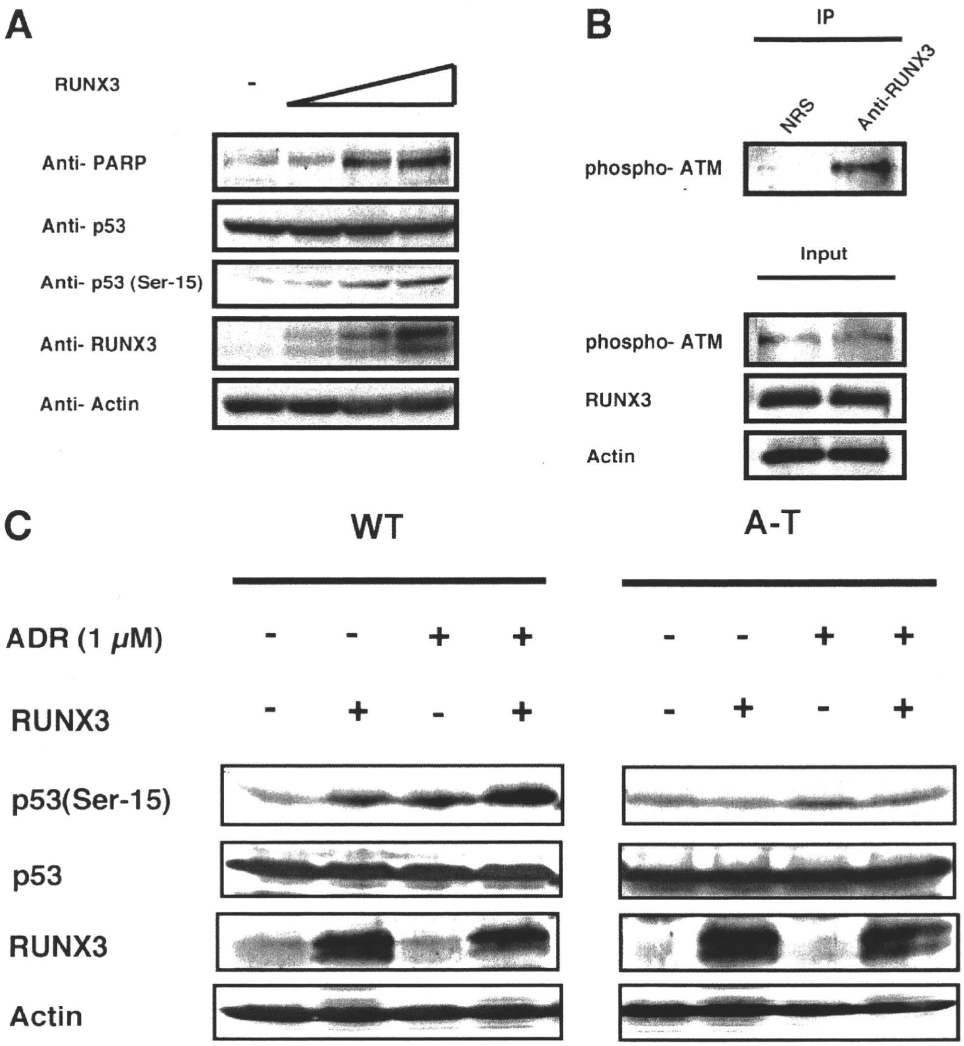

FIGURE 6. **RUNX3 induces phosphorylation of p53 at Ser-15 in an ATM-dependent manner.** *A*, RUNX3 induces phosphorylation of p53 at Ser-15. U2OS cells were transiently transfected with or without increasing amounts of RUNX3 expression plasmid. Forty eight hours after transfection, lysates were prepared and analyzed by immunoblotting with the indicated antibodies. *B*, RUNX3 interacts with phosphorylated forms of ATM. Lysates prepared from HeLa cells exposed to ADR at a final concentration of 1 μM were immunoprecipitated (*IP*) with normal rabbit serum (*NRS*) or with polyclonal anti-RUNX3 antibody followed by immunoblotting with anti-phospho-ATM antibody. *C*, RUNX3 enhances ADR-mediated phosphorylation of p53 at Ser-15. Wild-type (*WT*) and ATM-deficient A-T cells were transiently transfected with or without RUNX3 expression plasmid in the presence or absence of ADR at a final concentration of 1 μM. Lysates were subjected to immunoblotting with the indicated antibodies.

death in response to ADR in cells bearing wild-type *p53* but not in *p53*-deficient cells. Of note, knocking down of the endogenous *RUNX3* led to a significant inhibition of ADR-mediated phosphorylation of p53 at Ser-15 in association with a massive inhibition of p53-dependent up-regulation of several p53-target genes as well as proteolytic cleavage of PARP. Furthermore, RUNX3 was induced and translocated from the cytoplasm into the cell nucleus in response to ADR. Consistent with these observations, forced expression of RUNX3 promoted phosphorylation of p53 at Ser-15 and proteolytic cleavage of PARP, suggesting that RUNX3 contributes to the regulation of DNA damage-induced phosphorylation of p53 at Ser-15.

It has been established that DNA damage-mediated phosphorylation of ATM is an early event in transducing DNA damage signal (34). After the phosphorylation of ATM, the phosphorylated form of histone H2AX (γH2AX), which is mediated by phospho-ATM, marks a chromatin region at or near the sites of DNA damage (35). According to our present results, RUNX3 had a marginal effect on ADR-mediated phosphorylation level of ATM, whereas RUNX3 had an undetectable effect on the amounts of γH2AX in response to ADR, indicating that RUNX3 is not involved in the initial step of DNA damage response and also does not affect the extent of DNA damage. It is worth noting that phosphorylated forms of ATM are associated with RUNX3 as examined by immunoprecipitation experiments. Thus, it is likely that RUNX3 assists DNA damage-induced phosphorylation of p53 at Ser-15 through complex formation with phosphorylated forms of ATM and enhances transcriptional as well as pro-apoptotic activity of p53, although Khanna *et al.* (36) reported that ATM directly binds to and phosphorylates p53 at Ser-15.

As described previously (15, 37), RUNX3 had an ability to increase the expression levels of $p21^{WAF1}$ and pro-apoptotic Bim in collaboration with the activated Smad proteins during TGF-β-mediated apoptotic cell death. In addition, p300-mediated acetylation of RUNX3 resulted in an increase in its stability (15). So far, RUNX3 has been implicated in carcinogenesis as a nuclear effecter of TGF-β tumor suppressor pathway (14, 15) and as an attenuator of oncogenic Wnt signaling pathway (21). We found the third RUNX3-mediated pro-apoptotic pathway that includes functional interaction between RUNX3 and p53. These pathways might be chosen under certain conditions in the tissue- or lineage-specific progenitor or stem cells to suppress their malignant transformation.

Based on our present results, RUNX3 was able to enhance the transactivation and pro-apoptotic activities of p53. Indeed, RUNX3 enhanced the p53-mediated up-regulation of $p21^{WAF1}$, *BAX*, and *PUMA*. Our extensive immunoprecipitation and *in vitro* pulldown assays revealed that the extreme COOH-terminal portion of p53 is required for the interaction with RUNX3. Initial studies suggest that the COOH-terminal region of p53 acts as a negative regulator and might lock its DNA-binding domain in a latent conformation (38, 39). However, this model has been challenged by the findings showing that stress-induced acetylation of COOH-terminal Lys-373 and Lys-382 of

p53 is required for the transcriptional activity of p53 (40). Additionally, this COOH-terminal acetylation resulted in an inhibition of p53 ubiquitination (40). Furthermore, McKinney *et al.* (41) described that the COOH-terminal region of p53 might facilitate the search for specific target sequences in the context of a complex genome. These results indicate that the COOH-terminal region of p53 is a positive regulator of DNA binding and transactivation. In support of this notion, COOH-terminally truncated splice variant, p53β, lacked the transactivation function (42, 43). It remains unclear how RUNX3 could contribute to the activation of p53 through its binding to the COOH-terminal region of p53. Further studies should be required to address this issue.

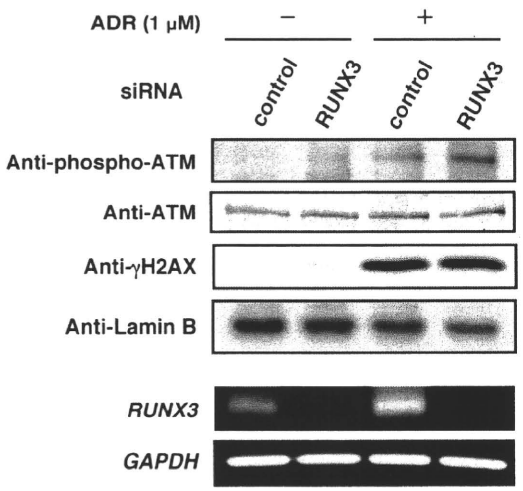

FIGURE 7. **Effect of silencing of RUNX3 on ADR-mediated phosphorylation of ATM and histone H2AX.** U2OS cells were transiently transfected with control siRNA or with siRNA targeting RUNX3. Twenty four hours after transfection, cells were treated with 1 μM ADR or left untreated. Twenty four hours after ADR treatment, nuclear lysates and total RNA were subjected to immunoblotting and RT-PCR, respectively. For immunoblotting, lamin B was used as a loading control. For RT-PCR, *GAPDH* was used as an internal control.

Another important finding of this study was that RUNX3 affects the phosphorylation status of p53, whereas RUNX3 has undetectable effect on its stability. Based on our present results, siRNA-mediated knockdown of the endogenous *RUNX3* and forced expression of RUNX3 had a negligible effect on the stability of p53. However, RUNX3 enhanced the p53-mediated transcriptional and pro-apoptotic activities. Although the accumulating evidence strongly suggests that DNA damage-induced accumulation and phosphorylation of p53 correlates with a significant increase in its activity (20), it is conceivable that DNA damage-induced stabilization of p53 might be a distinct phenomenon from DNA damage-mediated phosphorylation at Ser-15 and activation of p53 in certain experimental systems. In support of this notion, Ashcroft *et al.* (29) demonstrated that DNA damage-induced stabilization of p53 is observed irrespective of its phosphorylation status.

As described previously (15), TGF-β treatment led to a nuclear translocation of RUNX3 and induced apoptotic cell death through the transactivation of pro-apoptotic *Bim*. In a good agreement with these observations, RUNX3 was inactivated through its mislocalization to cytoplasm (17, 18). Under our experimental conditions, exogenously expressed RUNX3 was localized both in the cytoplasm and cell nucleus in the absence of DNA damage as examined by indirect immunofluorescence staining and immunoblotting experiments. It was worth noting that ADR treatment induces a significant nuclear translocation of RUNX3 and RUNX3 is co-localized with p53 in cell nucleus. Collectively, our present study strongly suggests that RUNX3 contributes at least in part to p53-mediated apoptotic cell death in response to DNA damage through the regulation of p53 phosphorylation at Ser-15.

In addition, our clinical study using primary human lung adenocarcinoma tissues suggested that patients with low expression of *RUNX3* and *p53* mutation display the poor prognosis. Thus, it is likely that the RUNX3/p53 pro-apoptotic pathway might be disrupted in the advanced stages of lung adenocarci-

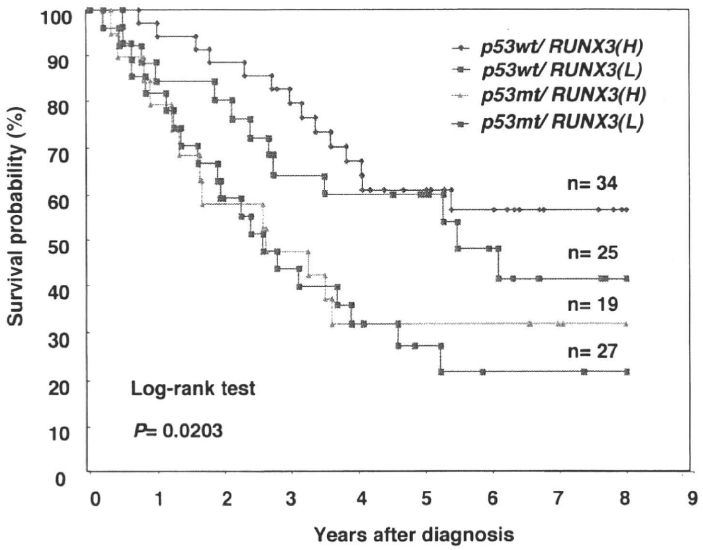

Stage	*p53wt/ RUNX3(H)*	*p53wt/ RUNX3(L)*	*p53mt/ RUNX3(H)*	*p53mt/ RUNX3(L)*
I	18 (53 %)	11 (44 %)	9 (47 %)	2 (7 %)
II-IV	16 (47 %)	14 (56 %)	10 (53 %)	25 (93 %)

Fisher's exact test, *P*= 0.0018; wt: wild-type, mt: mutant, H: high expression, L: low expression

FIGURE 8. **Combination of *p53* mutation and low expression levels of *RUNX3* is associated with poor prognosis of patients with lung adenocarcinoma.** Cumulative survival curves of 105 patients with lung adenocarcinoma based on wild-type *p53* (*p53wt*) or mutant (*p53mt*) and high (*H*) or low (*L*) expression of *RUNX3* analyzed by a quantitative real time RT-PCR (top) are shown. Number of patients divided by *p53* status and expression levels of *RUNX3* was categorized based on the clinical stage (I or II–V) of the patient (bottom). *p* values were calculated according to the indicated statistical analysis.

noma. Further precise understandings of molecular mechanisms behind the collaboration of RUNX3 with p53 may provide a clue for developing novel diagnostic tools and therapeutic strategies against high risk cancers.

Acknowledgments—We are grateful to M. Ohira, S. Fujimoto, and M. Yamamoto for examining p53 mutations and measuring RUNX3 mRNA expression in lung cancers.

REFERENCES

1. Ito, Y. (2008) *Adv. Cancer Res.* **99,** 33–76
2. Okuda, T., van Deursen, J., Hiebert, S. W., Grosveld, G., and Downing, J. R. (1996) *Cell* **84,** 321–330
3. Look, A. T. (1997) *Science* **278,** 1059–1064
4. Komori, T., Yagi, H., Nomura, S., Yamaguchi, A., Sasaki, K., Deguchi, K., Shimizu, Y., Bronson, R. T., Gao, Y. H., Inada, M., Sato, M., Okamoto, R., Kitamura, Y., Yoshiki, S., and Kishimoto, T. (1997) *Cell* **89,** 755–764
5. Otto, F., Thornell, A. P., Crompton, T., Denzel, A., Gilmour, K. C., Rosewell, I. R., Stamp, G. W., Beddington, R. S., Mundlos, S., Olsen, B. R., Selby, P. B., and Owen, M. J. (1997) *Cell* **89,** 765–771
6. Li, Q. L., Ito, K., Sakakura, C., Fukamachi, H., Inoue, K., Chi, X. Z., Lee, K. Y., Nomura, S., Lee, C. W., Han, S. B., Kim, H. M., Kim, W. J., Yamamoto, H., Yamashita, N., Yano, T., Ikeda, T., Itohara, S., Inazawa, J., Abe, T., Hagiwara, A., Yamagishi, H., Ooe, A., Kaneda, A., Sugimura, T., Ushijima, T., Bae, S. C., and Ito, Y. (2002) *Cell* **109,** 113–124
7. Yanagawa, N., Tamura, G., Oizumi, H., Takahashi, N., Shimazaki, Y., and Motoyama, T. (2003) *Cancer Sci.* **94,** 589–592
8. Li, Q. L., Kim, H. R., Kim, W. J., Choi, J. K., Lee, Y. H., Kim, H. M., Li, L. S., Kim, H., Chang, J., Ito, Y., Youl Lee, K., and Bae, S. C. (2004) *Biochem. Biophys. Res. Commun.* **314,** 223–228
9. Kim, T. Y., Lee, H. J., Hwang, K. S., Lee, M., Kim, J. W., Bang, Y. J., and Kang, G. H. (2004) *Lab. Invest.* **84,** 479–484
10. Goel, A., Arnold, C. N., Tassone, P., Chang, D. K., Niedzwiecki, D., Dowell, J. M., Wasserman, L., Compton, C., Mayer, R. J., Bertagnolli, M. M., and Boland, C. R. (2004) *Int. J. Cancer* **112,** 754–759
11. Ku, J. L., Kang, S. B., Shin, Y. K., Kang, H. C., Hong, S. H., Kim, I. J., Shin, J. H., Han, I. O., and Park, J. G. (2004) *Oncogene* **23,** 6736–6742
12. Wada, M., Yazumi, S., Takaishi, S., Hasegawa, K., Sawada, M., Tanaka, H., Ida, H., Sakakura, C., Ito, K., Ito, Y., and Chiba, T. (2004) *Oncogene* **23,** 2401–2407
13. Kang, G. H., Lee, S., Lee, H. J., and Hwang, K. S. (2004) *J. Pathol.* **202,** 233–240
14. Zong, W. X., Lindsten, T., Ross, A. J., MacGregor, G. R., and Thompson, C. B. (2001) *Genes Dev.* **15,** 1481–1486
15. Yano, T., Ito, K., Fukamachi, H., Chi, X. Z., Wee, H. J., Inoue, K., Ida, H., Bouillet, P., Strasser, A., Bae, S. C., and Ito, Y. (2006) *Mol. Cell. Biol.* **26,** 4474–4488
16. Yamamura, Y., Lee, W. L., Inoue, K., Ida, H., and Ito, Y. (2006) *J. Biol. Chem.* **281,** 5267–5276
17. Ito, K., Liu, Q., Salto-Tellez, M., Yano, T., Tada, K., Ida, H., Huang, C., Shah, N., Inoue, M., Rajnakova, A., Hiong, K. C., Peh, B. K., Han, H. C., Ito, T., Teh, M., Yeoh, K. G., and Ito, Y. (2005) *Cancer Res.* **65,** 7743–7750
18. Lau, Q. C., Raja, E., Salto-Tellez, M., Liu, Q., Ito, K., Inoue, M., Putti, T. C., Loh, M., Ko, T. K., Huang, C., Bhalla, K. N., Zhu, T., Ito, Y., and Sukumar, S. (2006) *Cancer Res.* **66,** 6512–6520
19. Jin, Y. H., Jeon, E. J., Li, Q. L., Lee, Y. H., Choi, J. K., Kim, W. J., Lee, K. Y., and Bae, S. C. (2004) *J. Biol. Chem.* **279,** 29409–29417
20. Vousden, K. H., and Lu, X. (2002) *Nat. Rev. Cancer* **2,** 594–604
21. Melino, G., De Laurenzi, V., and Vousden, K. H. (2002) *Nat. Rev. Cancer* **2,** 605–615
22. Pietenpol, J. A., Tokino, T., Thiagalingam, S., el-Deiry, W. S., Kinzler, K. W., and Vogelstein, B. (1994) *Proc. Natl. Acad. Sci. U.S.A.* **91,** 1998–2002
23. Hollstein, M., Sidransky, D., Vogelstein, B., and Harris, C. C. (1991) *Science* **253,** 49–53
24. Levine, A. J., Chang, A., Dittmer, D., Notterman, D. A., Silver, A., Thorn, K., Welsh, D., and Wu, M. (1994) *J. Lab. Clin. Med.* **123,** 817–823
25. Ikawa, S., Nakagawara, A., and Ikawa, Y. (1999) *Cell Death Differ.* **6,** 1154–1161
26. Donehower, L. A., Harvey, M., Slagle, B. L., McArthur, M. J., Montgomery, C. A., Jr., Butel, J. S., and Bradley, A. (1992) *Nature* **356,** 215–221
27. Scheffner, M., Huibregtse, J. M., Vierstra, R. D., and Howley, P. M. (1993) *Cell* **75,** 495–505
28. Thomas, M. C., and Chiang, C. M. (2005) *Mol. Cell* **17,** 251–264
29. Ashcroft, M., Kubbutat, M. H., and Vousden, K. H. (1999) *Mol. Cell. Biol.* **19,** 1751–1758
30. Allan, L. A., and Fried, M. (1999) *Oncogene* **18,** 5403–5412
31. Furuya, K., Ozaki, T., Hanamoto, T., Hosoda, M., Hayashi, S., Barker, P. A., Takano, K., Matsumoto, M., and Nakagawara, A. (2007) *J. Biol. Chem.* **282,** 18365–18378
32. Yoshida, K., Ozaki, T., Furuya, K., Nakanishi, M., Kikuchi, H., Yamamoto, H., Ono, S., Koda, T., Omura, K., and Nakagawara, A. (2008) *Oncogene* **27,** 1183–1188
33. Ito, K., Lim, A. C., Salto-Tellez, M., Motoda, L., Osato, M., Chuang, L. S., Lee, C. W., Voon, D. C., Koo, J. K., Wang, H., Fukamachi, H., and Ito, Y. (2008) *Cancer Cell* **14,** 226–237
34. Shiloh, Y. (2003) *Nat. Rev. Cancer* **3,** 155–168
35. Paull, T. T., Rogakou, E. P., Yamazaki, V., Kirchgessner, C. U., Gellert, M., and Bonner, W. M. (2000) *Curr. Biol.* **10,** 886–895
36. Khanna, K. K., Keating, K. E., Kozlov, S., Scott, S., Gatei, M., Hobson, K., Taya, Y., Gabrielli, B., Chan, D., Lees-Miller, S. P., and Lavin, M. F. (1998) *Nat. Genet.* **20,** 398–400
37. Chi, X. Z., Yang, J. O., Lee, K. Y., Ito, K., Sakakura, C., Li, Q. L., Kim, H. R., Cha, E. J., Lee, Y. H., Kaneda, A., Ushijima, T., Kim, W. J., Ito, Y., and Bae, S. C. (2005) *Mol. Cell. Biol.* **25,** 8097–8107
38. Hupp, T. R., Meek, D. W., Midgley, C. A., and Lane, D. P. (1992) *Cell* **71,** 875–886
39. Friend, S. (1994) *Science* **265,** 334–335
40. Zhao, Y., Lu, S., Wu, L., Chai, G., Wang, H., Chen, Y., Sun, J., Yu, Y., Zhou, W., Zheng, Q., Wu, M., Otterson, G. A., and Zhu, W. G. (2006) *Mol. Cell. Biol.* **26,** 2782–2790
41. McKinney, K., Mattia, M., Gottifredi, V., and Prives, C. (2004) *Mol. Cell* **16,** 413–424
42. Bourdon, J. C., Fernandes, K., Murray-Zmijewski, F., Liu, G., Diot, A., Xirodimas, D. P., Saville, M. K., and Lane, D. P. (2005) *Genes Dev.* **19,** 2122–2137
43. Goldschneider, D., Horvilleur, E., Plassa, L. F., Guillaud-Bataille, M., Million, K., Wittmer-Dupret, E., Danglot, G., de Thé, H., Bénard, J., May, E., and Douc-Rasy, S. (2006) *Nucleic Acids Res.* **34,** 5603–5612

Biochemical and Biophysical Research Communications 392 (2010) 252–257

Contents lists available at ScienceDirect

Biochemical and Biophysical Research Communications

journal homepage: www.elsevier.com/locate/ybbrc

LMO3 interacts with p53 and inhibits its transcriptional activity

Steven Larsen, Tomoki Yokochi, Eriko Isogai, Yohko Nakamura, Toshinori Ozaki, Akira Nakagawara *

Division of Biochemistry and Innovative Cancer Therapeutics, Chiba Cancer Center Research Institute, Chiba, Japan

ARTICLE INFO

Article history:
Received 1 December 2009
Available online 6 December 2009

Keywords:
LMO3
p53
LIM-only protein
Tumor suppressor
Oncogene
Neuroblastoma

ABSTRACT

High expression of LMO3 contributes to the development and aggressiveness of neuroblastoma. LMO3 belongs to the LIM-only protein family, in which de-regulation of its members is implicated in human carcinogenesis. However, the molecular mechanism of LMO3 activity in oncogenesis remained poorly characterized. We found that LMO3 is a direct interacting partner of p53 both *in vitro* and *in vivo*. The DNA-binding domain of p53 is required for this interaction. Furthermore, expression of LMO3 repressed p53-dependent mRNA expression of its target genes by suppressing promoter activation. Interestingly, chromatin immunoprecipitation assay showed that LMO3 facilitated p53 binding to its response elements. This suggests that LMO3 acts as a co-repressor of p53, suppressing p53-dependent transcriptional regulation without inhibition of its DNA-binding activity.

Introduction

Cancer is predominantly a genetic disease. Alterations in genes controlling cell growth, survival and apoptosis are most commonly implicated in carcinogenesis. Our knowledge of cancer biology and medicine is currently increasing at an exponential rate, yet the transition to clinical applications is progressing much slower. Therefore, new targets and pathways need to be identified, particularly those having clinical significance and with the potential for specific and novel therapeutic applications at the bedside. Neuroblastoma is one of the most common childhood cancers and is originated from sympathoadrenal lineage of the neural crest [1]. The bulk of sporadic neuroblastomas are detected at advanced stage with poor survival rates of less than 40%, despite intensive multimode therapy [2]. Often, initial therapy appears effective but is frequently followed by the appearance of drug resistance, with frequent acquisition of p53-mutations.

The tumor suppressor p53 is one of the key tumor suppressors protecting against cancer and genetic abnormalities, with mutations in over half of all human cancers [3]. In fact, the bulk of p53 mutations occur in the DNA-binding domain affecting the ability of p53 to act as an effective transcription factor [4]. High levels of *p53* mRNA are described for neuroblastoma cell lines, yet p53 mutations are reported in less than 2% of neuroblastomas compared with up to 60% in other cancers. p53 is thought to be inactivated by alternative mechanisms. In fact, the subject of p53 inactivation is one of the most controversial topics in neuroblastoma research [5].

The nuclear LIM-only proteins consist of four members, LMO1, LMO2, LMO3, and LMO4. They are twin LIM-domain containing proteins that mediate protein–protein interactions, which can bind to transcription factors forming a DNA-binding complex. Despite strong links with transcriptional regulation, no DNA-binding activity has been found. They demonstrated decisive roles in distinct developmental pathways and that de-regulation of their expression is linked to oncogenesis [6–8]. De-regulation of LIM-only protein family members have been implicated in various cancers. Transgenic mice for the founding members, LMO1 and LMO2, developed immature and aggressive T-cell leukemia [9]. The more recently discovered LMO-family member, LMO4, is implicated in the cause and progression of human breast cancers [10], sqaumous cell carcinomas of the oral cavity [11] and primary prostate cancers [12]. LMO3 binding to its interacting partners is involved in cell fate determination of the sympathoadrenal lineage and is closely related to development of neuroblastoma [6,13,14]. Double knockout mice for *LMO1* and *LMO3* demonstrated a lethal phenotype [6]. Bao et al. [13] reported the cooperation of *Xenopus* HEN1 with XLMO3 as a critical regulator of neurogenesis. In the case of LMO1, the LIM domain shares 98% homology with LMO3 [6,14,15] and demonstrates redundancy in murine *in vivo* studies, in which double mutants of *LMO1* and *LMO3* transgenic mice exhibited perinatal death. Whereas, single mutants of either of these genes developed with an apparently normal phenotype [6]. Additionally, several oncogenic characteristics arising from LMO3 expression have been identified, both *in vitro* and *in vivo*. These include increased cell proliferation in normal and low serum conditions, colony formation in soft agar and rapid tumor growth in

* Corresponding author. Address: Division of Biochemistry and Innovative Cancer Therapeutics, Chiba Cancer Center Research Institute, 666-2 Nitona, Chuou-ku, Chiba 260-8717, Japan. Fax: +81 43 265 4459.
E-mail address: akiranak@chiba-cc.jp (A. Nakagawara).

0006-291X/$ - see front matter © 2009 Elsevier Inc. All rights reserved.
doi:10.1016/j.bbrc.2009.12.010

nude mice of SH-SY5Y cells stably expressing LMO3 [14]. High levels of *LMO3* mRNA were found in aggressive neuroblastomas with a poor prognosis as compared with more favorable subtypes [14]. In our previous report, analysis of cDNA libraries from different subsets of neuroblastoma and cloning of 4200 genes identified *LMO3* as being differentially expressed in neuroblastoma [15]. Clinical studies revealed that low expression of *LMO3* correlated with a favorable probability of survival and high expression with a much poorer prognosis [14].

The molecular mechanisms of LMO3 activity in oncogenesis remain poorly characterized and the potential for inhibition of tumor suppressors has not been investigated to date. The novel finding presented here is that LMO3 can function as an oncogene by binding to and inhibiting the key tumor suppressor p53, which results in reduced transcription of apoptosis-related genes.

Materials and methods

Cell lines and transfection assays. Small cell lung carcinoma, H1299 and African green monkey, COS-7 mammalian cells were maintained at 37 °C/5% CO_2 in either RPMI 1640 or DMEM supplemented with 10% heat inactivated fetal bovine serum, 100 IU/ml penicillin and 100 μg/ml streptomycin. Where indicated, cells were transfected using either LipofectAMINE 2000 (Invitrogen, CA, USA) or FuGene HD (Roche Applied Science, IN, USA) transfection reagents according to manufacturer recommendations. Total amount of transfected plasmid DNA was adjusted to constant levels with empty parental pcDNA3 plasmid (Invitrogen).

Immunoprecipitation and GST-pull down assays. Immunoprecipitation was essentially performed as in [16] using anti-p53 (DO-1, Calbiochem, CA, USA; pab1801, Santa Cruz Biotechnology, CA, USA) monoclonal antibodies; or anti-flag tag (M2; Sigma, MI, USA) monoclonal antibody. Immunoprecipitated proteins were resolved by SDS–PAGE and detected by immunoblotting.

For the *in vitro* GST-pull down experiments, plasmid constructs encoding the p53 deletion mutants, p53 (1–359), p53 (1–292), p53 (1–102) and p53 (102–393) were used to create the respective [^{35}S]-methionine labeled proteins by an *in vitro* coupled transcription/translation system (Promega, WI, USA). GST only or GST-LMO3 fusion protein was produced by induction with isopropyl β-D-1-thiogalactopyranoside (IPTG) and expression in bacteria and purified with Glutathione Sepharose beads. Expression efficiency and purification was checked by Coomassie Brilliant Blue R-250 (CBB) staining and western blot analysis. Approximately equimolar amounts (determined by SDS–PAGE) of GST or GST-LMO3 fusion proteins were immobilized on glutathione-Sepharose beads and incubated with *in vitro* translated p53 deletion mutants, essentially as described in [17]. The bound [^{35}S]-methionine labeled proteins were resolved by 12% SDS–PAGE, incubation with Amplify (Amersham, Chalfont, UK) enhancer reagent and detected by autoradiography.

Semi-quantitative RT-PCR. Total RNA was isolated and purified from cultured cells using the RNeasy kit (Qiagen, Hilden, Germany). The RNA concentration was calculated and equal amounts were reverse transcribed using SuperScript II reverse transcriptase and random primers (Invitrogen). The resultant cDNA was subject to PCR-based amplification with gene-specific primers (sequences are available on request).

Indirect immunofluorescence. H1299 cells were grown on sterile coverslips 1 day prior to transfection with p53 and FLAG-LMO3 expression constructs, then slides prepared for immunofluorescence microscopy as described in [18]. Cells were incubated with a mixture of polyclonal anti-FLAG epitope and monoclonal anti-p53 (DO-1; Calbiochem) primary antibodies and fluorescein isothiocyanate- (FITC) or Rhodamine-conjugated secondary antibodies. Cover slips were mounted onto glass slides using 4,6-diamidino-2-phenylindole dihydrochloride (DAPI) containing Vector Shield mounting medium (Vector Laboratories, CA, USA) and imaged using fluorescence microscopy and Image Ready Easy software.

Luciferase gene reporter assay. H1299 cells plated in a 12-well plate were allowed to adhere overnight and then transfected with indicated reporter constructs and *Renilla* luciferase by LipofectAMINE 2000 (Invitrogen). Total amount of transfected DNA was kept constant with empty pcDNA3 plasmid. Both *Renilla* and firefly luciferase activity were assayed at 36 h post-transfection using the dual-luciferase reporter assay system (Promega). Firefly gene reporter activity was calculated relative to *Renilla* luminescence.

Chromatin immunoprecipitation. Chromatin immunoprecipitation assays were performed using reagents and the protocol provided by Upstate Biotechnology (NY, USA), with the modification that purification of de-crosslinked DNA was performed using QIAquick PCR purification kit (Qiagen). Purified DNA was analyzed by PCR-based amplification of p53 responsive elements of *p21*, *bax*, and *puma* promoters using the specific primers as follows: *p21*, 5′-gagcctccctccatccctat-3′ (forward), 5′-ctgctgcccaagcatgttc-3′ (reverse); *bax*, 5′-cggtagctcatgcctgtaatcc-3′ (forward), 5′-aacttgtgagcccaagagataacc-3′ (reverse); *puma*, 5′-gccttgtgtctgtgagtacatcct-3′ (forward), 5′-gttccagggtccacaaagtca-3′ (reverse).

Immunoblotting and antibodies. Equivalent amounts of protein lysates normalized to actin levels were separated by SDS–PAGE, transferred to a polyvinylidene fluoride membrane (Millipore, MA, USA). The membrane was probed with anti-p53 (DO-1; Calbiochem), anti-phospho ser 15 p53 (Cell Signalling Technology, MA, USA) anti-FLAG tag (M2; Sigma), anti-HA tag (6E2; Cell Signalling Technology), anti-actin (Sigma), anti-PARP (Cell Signalling Technology) antibody followed by incubation with horseradish peroxidase conjugated goat anti-mouse or anti-rabbit secondary antibody (Cell Signalling Technology). Immunoblots were visualized by enhanced chemoluminescence reagents (Amersham) and exposed to X-ray film.

Results

Physical interaction between LMO3 and the DNA-binding domain of p53

LMO3 was previously described as an oncogene in neuroblastoma [14] and mutations of p53 are rarely found in this childhood cancer. However, the p53 tumor suppressor is thought to be inactivated by alternative pathways. Furthermore, binding to and inhibition of tumor suppressors are reported for other LIM-only protein family members. Additionally, LIM-only proteins are involved in protein–protein interactions and known to act as cofactors in DNA-binding complexes. Considering these facts, we examined a potential relationship between LMO3 and the p53 pathway. Towards this aim, we used indirect immunofluorescence to identify the subcellular distributions of LMO3 and p53 (Fig. 1A). LMO3 protein (green) was predominantly localized in the cell nucleus (blue), indicating that LMO3 is principally a nuclear protein when expressed in p53-null H1299 cells. Merged images of LMO3 and p53 (red) staining revealed co-localization in the cell nucleus. These observations suggested a possible association of LMO3 with p53 in the cell nucleus.

Leading on from the co-localization experiments, *in vitro* and *in vivo* binding studies were performed (Fig. 1B–1E). Cell lysates prepared from H1299 cells co-transfected with p53 and LMO3 were subjected to immunoprecipitation with either an anti-FLAG (1B; left panel) or an anti-p53 (Fig. 1B; right panel). Immunoprecipitated proteins were detected by immunoblotting with anti-p53 and anti-FLAG antibodies, respectively. This suggests that

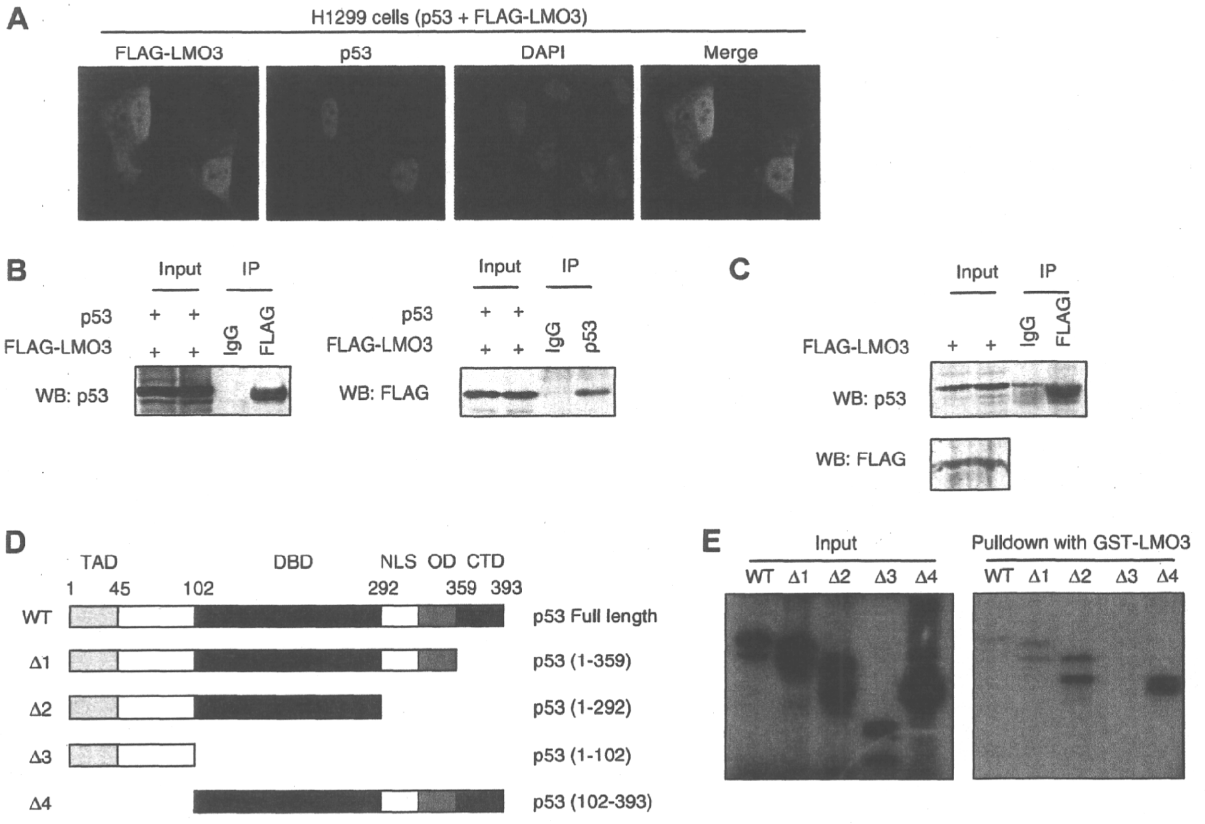

Fig. 1. Direct physical interaction of p53 and LMO3, requiring the DNA-binding domain of p53. (A) Co-localization of p53 and LMO3 in H1299 cells by indirect-immunofluorescence. Cells were transfected with p53 and FLAG-LMO3 expression vectors, and then incubated with a combination of anti-p53 (red) and polyclonal anti-FLAG (green) antibodies. The nuclei were visualized by DAPI staining (blue). (B) Either anti-FLAG (left panel) or anti-p53 (right panel) antibodies were used to prepare immunoprecipitates from H1299 cells co-transfected with p53 and FLAG-LMO3. These cells were treated with 10 μM MG132 8 h prior to harvest. Co-immunoprecipitated proteins were analyzed by western blotting. (C) Co-immunoprecipitation of endogenous p53 with FLAG-LMO3 antibody. (D) Schematic representation of p53 domain structures and deletion mutants used in this study. Amino acid residues are indicated by numbers. TAD, transactivation domain; DBD, DNA-binding domain; NLS, nuclear localization; OD, oligomerization domain; CTD, C-terminal regulatory domain. (E) p53 binding domain determination by *in vitro* GST-pull down assay. *In vitro* binding assay using translated ^{35}S labeled full length and deletion mutants of p53 are shown; input (left panel); pulldown with GST-LMO3 (right panel).

p53 and LMO3 proteins can physically interact, indicating the capacity of LMO3 to form a stable association with p53 in cells.

To confirm the binding of LMO3 with endogenous p53, whole cell lysate prepared from COS-7 cells transfected with FLAG-LMO3 was immunoprecipitated with anti-FLAG antibody (Fig. 1C) and then immunoblotted with anti-p53 antibody. Immunocomplexes containing endogenous p53 protein could be detected in anti-FLAG antibody immunoprecipitates for COS-7 cells expressing FLAG-tagged LMO3. Immunoprecipitation of cell lysates with normal mouse IgG did not contain LMO3 or p53. In these experiments, LMO3 could co-immunoprecipitate with p53, demonstrating a physical interaction between these two proteins in cells.

To examine this physical interaction in detail, we determined the essential region(s) of p53 responsible for this interaction. We carried out *in vitro* binding studies using recombinant p53 proteins constructed with a series of deletions [16], depicted in Fig. 1D. These constructs contain deletion of the C-terminal regulatory domain (CTD), nuclear localization domain (NLS), oligomerization domain (OD), DNA-binding domain (DBD) or transcriptionally active domain (TAD). The GST-LMO3 bead complex was incubated with radiolabeled p53 deletion mutants, generated by an *in vitro* transcription/translation system in the presence of [^{35}S]-methionine (Fig. 1E; left panel). GST-LMO3 could pull down all of the p53 deletion mutants, with the exception of p53 (1–102). This result implies that the region between amino acid residues 102 and 292 of p53 (DBD) is required for the physical interaction with LMO3 (Fig. 1E; right panel), suggesting that LMO3 directly binds to the DNA-binding domain of p53.

LMO3 demonstrates repressor activity on p53-mediated transcriptional activation

The functional significance of this LMO3-p53 interaction was investigated by assessing the ability of p53 to activate its target gene expression. Detection of endogenous mRNAs by RT-PCR was used to assess the effect of LMO3 expression on the transcriptional ability of p53 (Fig. 2A). H1299, a p53-null cell line, was co-transfected with constant amount of p53 expression plasmid and increasing amount of LMO3 plasmid. Expression of LMO3 repressed p53-mediated induction of its target genes, such as $p21^{WAF1}$, *Noxa*, *Bax*, and *Puma*. Endogenous mRNAs were repressed in a dose-dependent manner by co-expression of LMO3 (Fig. 2A). Constant expression of p53 and dose dependent expression of LMO3 were confirmed by RT-PCR. To further confirm this transcriptional repression, we utilized a firefly/*Renilla* luciferase gene reporter assay to analyze promoter activation of p53 target genes. Luciferase gene reporter constructs possessing the $p21^{WAF1}$, *Bax*, or *Mdm2* promoter regions were transfected into H1299 cells, together with or without increasing amounts of FLAG-LMO3 expression plasmid and a constant amount of p53. Enforced Plk1 expression was previously reported to inhibit the transcriptional activity of p53 [16] and therefore used to verify our results. As indicated in Fig. 2B,

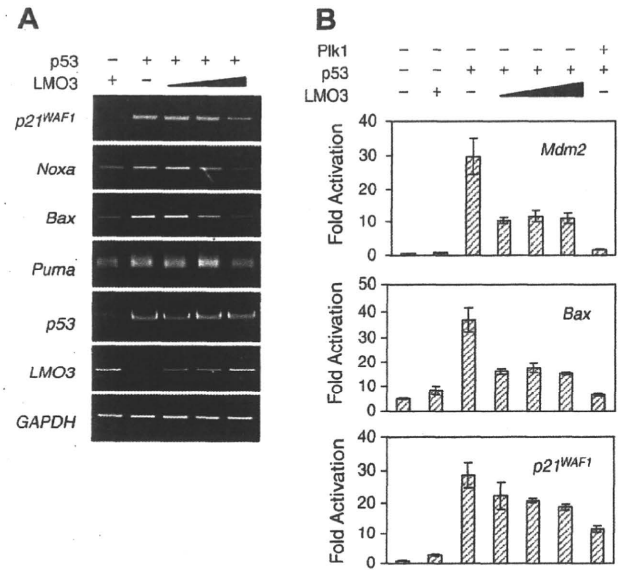

Fig. 2. LMO3 inhibits the transcriptional ability of p53. (A) mRNA levels of p53 target genes following p53 overexpression in p53-deficient H1299 cells, with co-expression of an increasing amount of LMO3 plasmid. Total RNA was extracted and subjected to RT-PCR analysis of *Noxa*, *Bax*, $p21^{WAF1}$ and *Puma*; detection of *GAPDH* was used as a loading control. (B) Luciferase gene reporter assay of $p21^{WAF1}$, *Bax* and *Mdm2* promoter regions. H1299 cells were transiently transfected with the indicated combination of p53 and increasing LMO3 plasmid. Results are the mean of three independent experiments ± standard deviation.

p53-mediated activation of $p21^{WAF1}$, *Bax*, and *Mdm2* promoter regions was reduced by co-expression of FLAG-LMO3 when compared to transfection of p53 alone. Therefore, both endogenous mRNA transcription and activation of p53-responsive promoter elements were reduced upon co-expression with LMO3. These findings signify that LMO3 acts as a co-repressor of p53, suppressing p53-mediated transcriptional regulation.

Promoter recruitment of p53 is affected by LMO3

We attempted to clarify the mechanism by which LMO3 represses p53-mediated gene activation. For this, we employed ChIP assays to characterize the recruitment of p53 onto p53-response elements in the *p21*, *Bax* and *Puma* promoters. Both p53 and LMO3 proteins could be expressed in H1299 cells, detected by western blot (Fig. 3A). This experimental system revealed that specific recruitment of exogenously expressed p53 onto the promoters of *p21*, *Bax*, and *Puma* genes in the presence or absence of HA-LMO3 (Fig. 3B). The specificity of the anti-p53 antibody to precipitate p53 bound chromatin is shown by the lack of PCR product in the absence of p53, LMO3 only transfection, and ChIP with normal mouse IgG. The effect of LMO3 on p53 recruitment to these regions appears to be promoter specific, as a clear increase in recruitment of p53 to the *p21* promoter was observed when LMO3 was present in cells. A similar tendency at *Bax* and *Puma* promoters was observed to a lesser extent.

Discussion

LMO3 can act as an oncogene by promoting cell survival when highly and abnormally expressed in neuroblastoma [14]. Furthermore, we report here that LMO3 inhibits p53, one of the key molecules in protection against cancer. This oncogenic action of LMO3 is comparable to the activity of other LIM-only protein family members against tumor suppressor proteins [19]. Additionally, the compensatory roles of LMO1 and LMO3 in development [6] suggest common mechanisms of activity between LIM-only proteins. Yet the timing of expression levels and topography result in subtly distinct outcomes. Taken together with our previous studies, recent results are consistent with the notion that LIM-only proteins are regulatory proteins which have essential functions in transcriptional regulation, while they can be potent oncogenes under conditions of abnormal expression.

We demonstrated that LMO3 represses p53-mediated activation and transcription of apoptosis-related genes. The loss of p53 activation provides tumor cells with several selective advantages, such as an increased tolerance to growth arrest and apoptosis-inducing protective mechanisms, in addition to genetic instability [3,5]. This indicates that p53 is either inactivated or repressed by LMO3, even though p53 still retains nuclear localization and DNA-binding capability. Additionally, activation of the DNA-damage response by CDDP treatment demonstrated a functioning p53 pathway in SH-SY5Y cells including the transcriptional activation of *p21* (**Supplementary Fig. 1**). Interestingly, p53 recruitment to the $p21^{WAF1}$ promoter was increased by LMO3 expression. However, in all p53-activated genes studied, LMO3 could repress their transcription by p53. Thus, LMO3 expression can influence p53 recruitment in a promoter selective manner but this may not be the main mechanism of repression.

As no enzymatic activity has been reported for LMO3, we propose that de-regulation of LMO3 expression leads to abnormal complex formation because of inappropriate LMO3 interactions. Our ChIP assay suggests that LMO3 does not suppress p53-mediated gene activation by interfering with DNA-binding. Therefore, another repression mechanism must exist. Accumulating evidence has demonstrated that post-translational modification of histones correlate with gene transcriptional regulation. Generally, Histone acetylation is associated with gene activation [20]. Physical and functional interactions of histone-acetyltransferases with p53, such as CBP and p300, demonstrate targeted acetylation of histones at promoter regions [21–23]. ChIP assays may indicate mod-

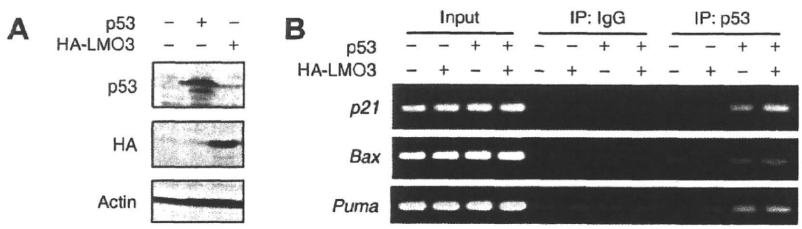

Fig. 3. Recruitment of p53 to promoters of apoptosis-related genes. (A) Immunoblotting showing expression of p53 and HA-LMO3 in p53-deficient H1299 cell line. (B) Chromatin immunoprecipitation with anti-p53 antibody or control mouse IgG in H1299 cells transfected with the indicated combinations of p53 and HA-LMO3 expression plasmids.

ification of histone acetylation by overexpression of LMO3 in the chromatin of p53-target genes. Future studies should examine the potential protein–protein interactions and the nature of LIM-only protein complexes involved in epigenetic modifications of chromatin.

The discrepancy between increased p53 recruitment and repression of gene activation could be explained by the following mechanisms. p53 receives a complex assortment of post-translational modifications including phosphorylation, ubiquitination, sumoylation, methylation and acetylation. These modifications affect many aspects of p53 status and activity, such as protein stability, DNA-binding activity, promoter selection and target-gene activation and/or repression. Regarding the repression of p53-mediated transcription by LMO3, we could not find any reduction in protein stability (data not shown) and DNA-binding activity of p53 to the *p21*, *bax*, and *puma* promoters. This suggests that LMO3 regulation of p53 may affect the association with its co-activators and repressors. It has been proposed that LIM-only proteins exert their effect by mediating protein–protein interactions and competing for interacting domains in the assembly of protein complexes [24,25]. Thus, LMO3 may directly compete for recruitment of negative transcriptional regulators to the p53 DNA-binding complex and promoter regions. Alternatively, LMO3 could recruit post-translational modifiers of p53 affecting transcriptional activation via an indirect mechanism. One other possibility, although not yet established for LIM-only proteins, is that binding by LMO3 affects the protein folding of p53, allowing recruitment to its response element yet interferes with assembly of the transcription machinery.

We expected that alterations in LMO3 transcriptional complexes have an inappropriate regulatory effect on downstream targets. Indeed, this is supported by our findings that the interaction of LMO3 with p53 represses p53-mediated transcription. This seems to be a common theme among LIM-only proteins. For example, LMO4 inhibits the transcriptional activity of BRCA1, a major tumor suppressor in breast cancers [10,19]. Intriguingly, Simonis et al. [26] found that *LMO3* is activated by chromosomal translocations of the T-cell receptor beta locus associated with T-cell lymphomas. In view of this study, the activities and molecular pathways of LMO3 activity identified here and in our previous report may be applicable to T-ALL. For future studies of LMO3, the regulation of gene expression itself needs to be clearly defined.

Long term survival, especially for those over 18 months of age for children with advanced neuroblastoma is currently unsatisfactory. Regardless of a myriad of treatments, recovery rates are poor. Present treatment regimes include surgery, radiation therapy, chemotherapy, retinoic acid and immunotherapy with anti-GD2 monoclonal antibody. Currently, in high risk groups (around half of all patients) overall survival is less than 40% [2]. There is an urgent necessity for specific therapies that can selectively eliminate cancer cells while limiting damage to normal cells and tissues. In particular, identification of novel targets and pathways through studies of abnormal gene expression, mutations, and genetic abnormalities in the various stages of neuroblastoma is crucial. Inhibition of LMO3 may be useful in treatment of presently difficult to treat neuroblastomas. The potential for interference of LIM-only protein multi-complexes and subsequent inhibition of normal and tumorigenic roles has been demonstrated using vector mediated expression of an anti-LMO2 single chain Fv antibody fragment [27,28]. Recent advances which will allow for individual gene profiling of tumors and the ability to design specific inhibitors may lead to a personalized treatment regime based on expression of individual oncogenes. Therefore, specific targeting of LMO3 in highly expressing tumors may simultaneously permit activation of the p53 pathway and inhibit LMO3-mediated pro-survival mechanisms.

Acknowledgments

This work was supported in part by a Grant-in-Aid from the Ministry of Health, Labour and Welfare for Third Term Comprehensive Control Research for Cancer, a Grant-in-Aid for Scientific Research on Priority Areas from the Ministry of Education, Culture, Sports, Science and Technology, Japan. A scholarship was awarded to S.L. from the Fujii medical foundation. The authors are grateful to Dr. Takehiko Kamijo for valuable discussion.

Appendix A. Supplementary data

Supplementary data associated with this article can be found, in the online version, at doi:10.1016/j.bbrc.2009.12.010.

References

[1] G.M. Brodeur, C. Azar, M. Brother, et al., Neuroblastoma. Effect of genetic factors on prognosis and treatment, Cancer 70 (1992) 1685–1694.
[2] J.M. Maris, M.D. Hogarty, R. Bagatell, et al., Neuroblastoma, Lancet 369 (2007) 2106–2120.
[3] B. Vogelstein, D. Lane, A.J. Levine, Surfing the p53 network, Nature 408 (2000) 307–310.
[4] J. Zhu, S. Zhang, J. Jiang, et al., Definition of the p53 functional domains necessary for inducing apoptosis, J. Biol. Chem. 275 (2000) 39927–39934.
[5] A.Y. Nikolaev, M. Li, N. Puskas, et al., Parc: a cytoplasmic anchor for p53, Cell 112 (2003) 29–40.
[6] E. Tse, A.J.H. Smith, S. Hunt, et al., Null mutation of the Lmo4 gene or a combined null mutation of the Lmo1/Lmo3 genes causes perinatal lethality, and Lmo4 controls neural tube development in mice, Mol. Cell. Biol. 24 (2004) 2063–2073.
[7] S. Arber, G. Halder, P. Caroni, Muscle LIM protein, a novel essential regulator of myogenesis, promotes myogenic differentiation, Cell 79 (1994) 221–231.
[8] T. Boehm, L. Foroni, Y. Kaneko, et al., The rhombotin family of cysteine-rich LIM-domain oncogenes: distinct members are involved in T-cell translocations to human chromosomes 11p15 and 11p13, Proc. Natl. Acad. Sci. USA 88 (1991) 4367–4371.
[9] Y. Yamada, A.J. Warren, C. Dobson, et al., The T cell leukemia LIM protein Lmo2 is necessary for adult mouse hematopoiesis, Proc. Natl. Acad. Sci. USA 95 (1998) 3890–3895.
[10] E.Y.M. Sum, D. Segara, B. Duscio, et al., Overexpression of LMO4 induces mammary hyperplasia, promotes cell invasion, and is a predictor of poor outcome in breast cancer, Proc. Natl. Acad. Sci. USA 102 (2005) 7659–7664.
[11] H. Mizunuma, J. Miyazawa, K. Sanada, et al., The LIM-only protein, LMO4, and the LIM domain-binding protein, LDB1, expression in squamous cell carcinomas of the oral cavity, Br. J. Cancer 88 (2003) 1543–1548.
[12] S. Mousses, L. Bubendorf, U. Wagner, et al., Clinical validation of candidate genes associated with prostate cancer progression in the CWR22 model system using tissue microarrays, Cancer Res. 62 (2002) 1256–1260.
[13] J. Bao, D.A. Talmage, L.W. Role, et al., Regulation of neurogenesis by interactions between HEN1 and neuronal LMO proteins, Development 127 (2000) 425–435.
[14] M. Aoyama, T. Ozaki, H. Inuzuka, et al., LMO3 interacts with neuronal transcription factor, HEN2, and acts as an oncogene in neuroblastoma, Cancer Res. 65 (2005) 4587–4597.
[15] M. Ohira, A. Morohashi, H. Inuzuka, et al., Expression profiling and characterization of 4200 genes cloned from primary neuroblastomas: identification of 305 genes differentially expressed between favorable and unfavorable subsets, Oncogene 22 (2003) 5525–5536.
[16] K. Ando, T. Ozaki, H. Yamamoto, et al., Polo-like kinase 1 (Plk1) inhibits p53 function by physical interaction and phosphorylation, J. Biol. Chem. 279 (2004) 25549–25561.
[17] N. Koida, T. Ozaki, H. Yamamoto, et al., Inhibitory role of Plk1 in the regulation of p73-dependent apoptosis through physical interaction and phosphorylation, J. Biol. Chem. 283 (2008) 8555–8563.
[18] H. Niizuma, Y. Nakamura, T. Ozaki, et al., Bcl-2 is a key regulator for the retinoic acid-induced apoptotic cell death in neuroblastoma, Oncogene 25 (2006) 5046–5055.
[19] E.Y.M. Sum, B. Peng, X. Yu, et al., The LIM domain protein LMO4 interacts with the cofactor CtIP and the tumor suppressor BRCA1 and inhibits BRCA1 activity, J. Biol. Chem. 277 (2002) 7849–7856.
[20] S.Y. Roth, J.M. Denu, C.D. Allis, Histone acetyltransferases, Annu. Rev. Biochem. 70 (2001) 81–120.
[21] N.A. Barlev, L. Liu, N.H. Chehab, et al., Acetylation of p53 activates transcription through recruitment of coactivators/histone acetyltransferases, Mol. Cell 8 (2001) 1243–1254.
[22] J.M. Espinosa, B.M. Emerson, Transcriptional regulation by p53 through intrinsic DNA/chromatin binding and site-directed cofactor recruitment, Mol. Cell 8 (2001) 57–69.
[23] W. An, J. Kim, R.G. Roeder, Ordered cooperative functions of PRMT1, p300, and CARM1 in transcriptional activation by p53, Cell 117 (2004) 735–748.

[24] J.L. Kadrmas, M.C. Beckerle, The LIM domain: from the cytoskeleton to the nucleus, Nat. Rev. Mol. Cell. Biol. 5 (2004) 920–931.
[25] H.P. Ostendorff, R.I. Peirano, M.A. Peters, et al., Ubiquitination-dependent cofactor exchange on LIM homeodomain transcription factors, Nature 416 (2002) 99–103.
[26] M. Simonis, P. Klous, I. Homminga, et al., High-resolution identification of balanced and complex chromosomal rearrangements by 4C technology, Nat. Methods 6 (2009) 837–842.
[27] C. Nam, M.N. Lobato, A. Appert, et al., An antibody inhibitor of the LMO2-protein complex blocks its normal and tumorigenic functions, Oncogene 27 (2008) 4962–4968.
[28] T. Tanaka, R.L. Williams, T.H. Rabbitts, Tumour prevention by a single antibody domain targeting the interaction of signal transduction proteins with RAS, EMBO J. 26 (2007) 3250–3259.

Published OnlineFirst August 18, 2010; DOI:10.1158/1078-0432.CCR-09-2660

Clinical Cancer Research

Meta-analysis of Neuroblastomas Reveals a Skewed *ALK* Mutation Spectrum in Tumors with *MYCN* Amplification

Sara De Brouwer, Katleen De Preter, Candy Kumps, et al.

Clin Cancer Res 2010;16:4353-4362. Published OnlineFirst August 18, 2010.

Published OnlineFirst August 18, 2010; DOI:10.1158/1078-0432.CCR-09-2660

Human Cancer Biology

Clinical Cancer Research

Meta-analysis of Neuroblastomas Reveals a Skewed *ALK* Mutation Spectrum in Tumors with *MYCN* Amplification

Sara De Brouwer[1], Katleen De Preter[1], Candy Kumps[1], Piotr Zabrocki[4], Michaël Porcu[4], Ellen M. Westerhout[6], Arjan Lakeman[6], Jo Vandesompele[1], Jasmien Hoebeeck[1], Tom Van Maerken[1], Anne De Paepe[1], Geneviève Laureys[2], Johannes H. Schulte[8], Alexander Schramm[8], Caroline Van Den Broecke[3], Joëlle Vermeulen[1], Nadine Van Roy[1], Klaus Beiske[9], Marleen Renard[5], Rosa Noguera[10], Olivier Delattre[11], Isabelle Janoueix-Lerosey[11], Per Kogner[12], Tommy Martinsson[13], Akira Nakagawara[14], Miki Ohira[14], Huib Caron[7], Angelika Eggert[8], Jan Cools[4], Rogier Versteeg[6], and Frank Speleman[1]

Abstract

Purpose: Activating mutations of the anaplastic lymphoma kinase (*ALK*) were recently described in neuroblastoma. We carried out a meta-analysis of 709 neuroblastoma tumors to determine their frequency and mutation spectrum in relation to genomic and clinical parameters, and studied the prognostic significance of *ALK* copy number and expression.

Experimental Design: The frequency and type of *ALK* mutations, copy number gain, and expression were analyzed in a new series of 254 neuroblastoma tumors. Data from 455 published cases were used for further in-depth analysis.

Results: *ALK* mutations were present in 6.9% of 709 investigated tumors, and mutations were found in similar frequencies in favorable [International Neuroblastoma Staging System (INSS) 1, 2, and 4S; 5.7%] and unfavorable (INSS 3 and 4; 7.5%) neuroblastomas ($P = 0.087$). Two hotspot mutations, at positions R1275 and F1174, were observed (49% and 34.7% of the mutated cases, respectively). Interestingly, the F1174 mutations occurred in a high proportion of *MYCN*-amplified cases ($P = 0.001$), and this combined occurrence was associated with a particular poor outcome, suggesting a positive cooperative effect between both aberrations. Furthermore, the F1174L mutant was characterized by a higher degree of autophosphorylation and a more potent transforming capacity as compared with the R1275Q mutant. Chromosome 2p gains, including the *ALK* locus (91.8%), were associated with a significantly increased *ALK* expression, which was also correlated with poor survival.

Conclusions: *ALK* mutations occur in equal frequencies across all genomic subtypes, but F1174L mutants are observed in a higher frequency of *MYCN*-amplified tumors and show increased transforming capacity as compared with the R1275Q mutants. *Clin Cancer Res; 16(17); 4353–62. ©2010 AACR.*

Neuroblastoma is the most common solid extracranial pediatric tumor, with an annual incidence of 1 in 100,000 children below the age of 15 years (1). Despite intensive multimodal treatment, neuroblastoma remains fatal in almost half of the unfavorable patients. Insights into the molecular pathogenesis of this disease are required for the development of less toxic and more effective molecular targeted therapy. Detailed studies of patterns of DNA copy number alterations have been instrumental in our understanding of the clinical and biological heterogeneity of this tumor. Three major genomic subtypes represent >80% of all cases, i.e., hyperploid neuroblastoma with whole chromosome gains and losses, near diploid neuroblastoma with 11q deletions and 17q gain, and *MYCN*-amplified neuroblastoma with 1p deletions and 17q gain (2–5). The discovery of rare but recurrent high-level amplification

Authors' Affiliations: [1]Center for Medical Genetics, [2]Department of Paediatric Haematology and Oncology, and [3]Department of Pathology, Ghent University Hospital, Ghent, Belgium; [4]Department of Molecular and Developmental Genetics, K.U.Leuven-VIB, and [5]Department of Paediatrics, University Hospital Leuven, Leuven, Belgium; [6]Department of Human Genetics, Academic Medical Center, University of Amsterdam, and [7]Department of Pediatric Oncology, Emma Children's Hospital, Academic Medical Center, Amsterdam, the Netherlands; [8]Division of Hematology and Oncology, University Children's Hospital Essen, Essen, Germany; [9]Department of Pathology, Rikshospitalet, Oslo, Norway; [10]Department of Pathology, Medical School of Valencia, University of Valencia, Valencia, Spain; [11]INSERM U830, Institut Curie, Paris, France; [12]Childhood Cancer Research Unit, Karolinska Institutet, Astrid Lindgren Children's Hospital, Stockholm, Sweden; [13]Department of Clinical Genetics, Gothenburg University, Gothenburg, Sweden; [14]Division of Biochemistry and Innovative Cancer Therapeutics, Chiba Cancer Center Research Institute, Chiba, Japan

Note: Supplementary data for this article are available at Clinical Cancer Research Online (http://clincancerres.aacrjournals.org/).

S. De Brouwer and K. De Preter contributed equally to this work.

Corresponding Author: Frank Speleman, Center for Medical Genetics (CMGG), Ghent University Hospital, De Pintelaan 185, B-9000 Ghent, Belgium. Phone: 32-9-332-2451; Fax: 32-9-332-6549; E-mail: franki.speleman@UGent.be.

doi: 10.1158/1078-0432.CCR-09-2660

Published OnlineFirst August 18, 2010; DOI:10.1158/1078-0432.CCR-09-2660

Translational Relevance

Our study yielded a number of important new insights with clinical implications. First, *ALK* mutations are present in similar frequencies in all clinical stages of neuroblastoma (low as well as high stages). Second, F1174 hotspot mutations are associated with *MYCN* amplification and their combined occurrence leads to fatal disease outcome in all (except one) patients. A possible cooperation between the F1174 mutation and *MYCN* amplification may have implications for targeted therapy. Third, F1174 mutations have a higher transforming capacity than R1275 mutations. Finally, chromosome 2 copy gain, including the *ALK* locus, is associated with an increased *ALK* expression that was found to be associated with a significantly worse outcome in the global population. These findings shed a new and more detailed light on the distribution of *ALK* mutations in neuroblastoma. This information may be of importance in the light of choice of risk-related therapy and development of future targeted therapies.

of the *ALK* gene and a genetic study of familial neuroblastomas led to the discovery of activating *ALK* mutations in neuroblastoma (6–10). The frequency of *ALK* mutations in primary neuroblastoma varied between 6% and 11% in the different studies (6–10). The relatively low number of mutations described in each of the individual studies has precluded a thorough analysis of the frequency and distribution of recurrent *ALK* mutations across the different genomic subtypes. Moreover, in the first published series, there was a significant bias towards analysis of high-stage tumors, thus preventing a more general assessment of frequency and distribution of mutations across different stages (6–8). In our current study, we screened an additional 254 neuroblastoma cases including all clinical stages and genomic subtypes. In a meta-analysis, these findings were combined with those from 455 published cases (8–10) for which genomic subtype and clinical information were available. This strategy enabled us to analyze the *ALK* mutation profile in relation to genomic and clinical data in 709 neuroblastomas, which revealed a distinct mutation spectrum in relation to genomic subtype. Two hotspot mutations, F1174L and R1275Q, were shown to induce ALK autophosphorylation and were able to transform interleukin-3 (IL-3)-dependent Ba/F3 cells into cytokine-independent growth. In addition, we evaluated *ALK* gene expression levels and showed that high *ALK* expression is correlated with poor survival.

Materials and Methods

Neuroblastoma patients and cell lines

In total, 254 primary untreated neuroblastoma tumors with a tumor percentage >60% were investigated, including 44 stage 1, 30 stage 2, 34 stage 3, 113 stage 4, and 33 stage 4S tumors [according to the International Neuroblastoma Staging System (INSS); ref. 11]. Patient information and genomic subtypes for 455 published tumors screened for *ALK* mutations were retrieved from the publications or were made available by the authors (Supplementary Table S1; refs. 8–10). In addition, 39 neuroblastoma cell lines were included. The cell lines were obtained from several sources (see Supplementary Table S2). All of the cell lines were genotyped by DNA fingerprinting (PowerPlex, Promega).

Genomic DNA was isolated using the Qiagen DNA isolation kit (Qiagen) or a standard proteinase K/SDS procedure.

ALK DNA sequence analysis

For the first tumor cohort (146 cases) and the 39 cell lines, all 29 *ALK* coding exons were analyzed, whereas the remaining 108 tumors were screened for only the tyrosine kinase domain. Constitutional DNA from blood samples was available and analyzed for 12 of the 17 patients with a mutation in the primary tumor. Exons were amplified from genomic DNA (primer information in Supplementary Table S3). PCR products were subjected to directional or bidirectional sequencing using BigDye Terminator V1.1/V3.1 Cycle Sequencing chemistry on an ABI3730XL sequencer (Applied Biosystems). Electropherograms were analyzed using Seqscape v2.5 software (Applied Biosystems).

Array comparative genomic hybridization copy number profiling

To determine DNA copy number alterations, array comparative genomic hybridization (arrayCGH) was done by using an in-house developed 1 Mb resolution bacterial artificial chromosome array (BAC) array (37 samples) as previously described (3) or by using a custom-designed 44K array enriched for regions with recurrent imbalances in neuroblastoma (1p, 2p, 3p, 11q, 17; 217 samples; Agilent Technologies). For the latter, 150 ng of tumor and reference DNA were labeled with Cy3 and Cy5, respectively (BioPrime ArrayCGH Genomic Labeling System, Invitrogen). Further processing was done according to the manufacturer's guidelines. Features were extracted using the feature extraction v10.1.0.0.0 software program and processed with an in-house developed visualization software arrayCGHbase (http://medgen.ugent.be/arrayCGHbase; ref. 12), including circular binary segmentation for scoring of DNA copy number alterations (13).

ALK gene expression data

Gene expression data were available for 440 tumors, comprising a published dataset of 251 tumors profiled on custom Agilent 44k arrays (ref. 14; downloaded from the EBI ArrayExpress database E-TABM-38), an unpublished dataset of 101 tumors profiled on the Human Exon 1.0 ST Affymetrix arrays (normalized and summarized at the transcript level using RMAsketch), and an unpublished

[15] Koster et al., submitted.

Published OnlineFirst August 18, 2010; DOI:10.1158/1078-0432.CCR-09-2660

dataset of 88 tumors profiled on the Affymetrix HG-U133plus2.0 platform (normalized using MAS5 and downloaded from the R2 database).[15] Importantly, analyses were done on sets of tumors profiled on the same platform. For Kaplan-Meier and log-rank analysis, *ALK* expression levels were digitalized using the median expression value as cutoff.

Tissue microarray and immunohistochemistry

For the establishment of a tissue microarray, three representative areas from each tumor were selected on H&E-stained slides from 70 formalin-fixed and paraffin-embedded primary untreated neuroblastoma tumors (Supplementary Table S4). Neuroblastoma tumors were classified according to the International Neuroblastoma Pathology Classification (INPC) scoring system (15), which divides tumors into undifferentiated, poorly differentiated, and differentiating. Of each tumor, three cores were punched into the recipient block. Immunohistochemistry was done using a monoclonal mouse anti-human CD246 ALK antibody (clone ALK1, Dako), and slides were scored for immunoreactive neuroblastoma cells where 0 meant no or weak staining intensity (<10% of the cells), 1 meant weak staining intensity (10-50% of the cells), 2 meant medium staining intensity (50-80% of the cells), and 3 meant high staining intensity (>80% of the cells). The medium score of the three punches was calculated for Kaplan-Meier and log-rank analysis.

Western blotting

Lysis of cells was done when the neuroblastoma cell lines reached 70% confluency. Total cell lysates (50 μg of protein) were analyzed by standard procedures (16) using anti-phospho-ALK (Tyr1604), anti-ALK (Cell Signaling), and anti-ERK2 (Santa Cruz) antibodies. The Aida Image Analyzer v.4.22 was used for quantification of Western blots.

Transformation assay

Ba/F3 cells were cultured in RPMI-1640 supplemented with 10% fetal bovine serum and 1 ng/mL murine IL-3 (Peprotech). *ALK* F1174L and *ALK* R1275Q constructs were generated by PCR, cloned into the retroviral vector pMSCV-neo (Clontech), and transduced in Ba/F3 cells. Experiments were done in triplicate. Transduced Ba/F3 cells were selected with G418 (500 μg/mL medium). The amount of viable cells was assayed on regular intervals. For proliferation curves, Ba/F3 cells were washed with PBS, and 5×10^5 cells were seeded in 5 mL medium without IL-3. Viable cells were counted using a Vi-CELL Cell Viability Analyzer (Beckman Coulter) on days 3, 5, 7, and 9.

Statistical analysis

Fisher's exact tests, Mann-Whitney tests, and correlation analyses were done using R (version 2.8.1). The R Survival package was used to generate Kaplan-Meier plots and to carry out log-rank analyses. Multivariate logistic regression analysis was done using the glm function (R-base package).

Results

ALK mutation analysis in 254 primary neuroblastoma tumors and 39 neuroblastoma cell lines

In a series of 254 sporadic, nonfamilial primary neuroblastoma tumors, a total of 17 *ALK* mutations (6.7%) and 2 *ALK* amplifications (0.8%) were identified (Supplementary Fig. S1). In a first series of 146 cases, all 29 *ALK* coding exons were analyzed but no mutations were found outside the tyrosine kinase domain. Therefore, only the tyrosine kinase domain was analyzed for the remaining 108 tumors. The most frequent mutations were located at residues R1275 and F1174, and were detected in 3.9% (10 of 254) and 2.0% (5 of 254) of the cases, respectively. A third recurrent but less frequent mutation affecting residue F1245 (6–9) was not detected in our series. One of the mutations previously reported in only one tumor was also detected as a single case in our series (Y1278S; ref. 10), thus providing further evidence for its contribution to neuroblastoma pathogenesis. In addition to the previously reported mutations we observed one new missense mutation, R1231Q. Sequence analysis of the constitutional DNA of 12 of 17 patients with an *ALK* mutation showed that these mutations were somatically acquired.

Mutation analysis was also done in 39 neuroblastoma cell lines. All mutations, except for one (D1091N in LAN-6), were exclusively found within the tyrosine kinase domain. Recurrent mutations were found in two cell lines that were previously not analyzed, STA-NB-8 and NB-14. All results of previously reported cell lines were in concordance with published results except for one (see Supplementary Table S1).

Meta-analysis of *ALK* mutations reveals an increased occurrence of the F1174 mutation in *MYCN*-amplified tumors

We carried out a meta-analysis on the new cohort of 254 cases together with 455 previously analyzed and published cases to relate the *ALK* mutations to clinical and genomic data (8–10; Table 1 and Supplementary Table S1). The 709 samples had in total 49 *ALK* mutations (6.9%). The two most frequently occurring mutations were the F1174 (34.7%) and R1275 mutations (49%; Supplementary Fig. S1). When the entire group of different *ALK* mutations was taken into account in the evaluation of the overall frequency of *ALK* mutations, no significant difference was observed for the frequency of mutations in favorable (INSS 1, 2, and 4S; 14 of 245, 5.7%) versus unfavorable (INSS 3 and 4; 33 of 440, 7.5%) neuroblastomas (Fisher's exact test $P = 0.087$). Mutation frequencies were also compared within different stages, *MYCN* status, or age, but no significant differences were found (see Table 1 for P values). However, when looking at the different types of mutations in relation to the clinical and genomic parameters, we noticed a skewed distribution for *MYCN*

Published OnlineFirst August 18, 2010; DOI:10.1158/1078-0432.CCR-09-2660

Table 1. Results of Fisher-exact analysis comparing the distribution of genomic alterations, age, stage, and genomic subgroup in cases with one of the frequent *ALK* mutations or amplification versus wild-type cases

	Amplification or mutation vs wild-type	Mutation vs wild-type	Amplification vs wild-type	F1174 versus wild-type	R1275 versus wild-type	F1174 versus R1275
MYCN status	2.05E-04*	7.74E-02†	6.49E-07*	1.16E-03*	6.09E-01	5.31E-02†
1p-deletion‡	9.94E-02†	8.21E-01	8.03E-02†	3.57E-01	7.68E-01	2.91E-01
3p-deletion‡	3.45E-02†	5.54E-02†	1.00E-00	1.00E-00	2.36E-01	1.00E-00
11q-deletion‡	5.45E-02†	8.19E-02†	1.00E-00	1.00E-00	2.09E-01	5.00E-01
2p-gain‡	7.98E-01	1.00E-00	1.00E-00	6.02E-01	1.00E-00	5.26E-01
17q-gain‡	6.85E-01	6.72E-01	1.00E-00	7.03E-01	1.00E-00	1.00E-00
Age (<> 1 year)	4.07E-01	4.47E-01	7.73E-01	8.09E-02†	6.58E-01	9.33E-02†
Stage	9.94E-02†	1.66E-01	4.64E-01	6.70E-01	4.56E-01	8.13E-01
Genomic subtype	9.32E-04*	9.35E-02†	5.04E-06*	2.20E-02*	7.71E-01	3.92E-01

NOTE: The last column gives the results of the comparison of the cases with the F1174 mutation versus cases with the R1275 mutation.

*$P < 0.05$.

†$P < 0.1$.

‡Data are based on two of the four datasets for which detailed arrayCGH data were available.

status in the F1174 mutated cases versus the tumors with wild-type *ALK* ($P = 0.001$; Fig. 1A and Table 1). *ALK* F1174 mutations were found in 1.3% of the *MYCN*-single copy tumors, compared with 6.1% of *MYCN*-amplified tumors. Of the 17 tumors with the F1174 mutation, 58.8% had *MYCN* amplification, compared with a frequency of *MYCN* amplification of 21.6% in the tumors with wild-type *ALK* (Fig. 1A). In contrast, the frequency of *MYCN* amplification was similar for R1275 mutated versus wild-type cases. As most cell lines were *MYCN* amplified, we sequenced 39 neuroblastoma cell lines to verify whether the association of F1174 with *MYCN* amplification could also be detected. Indeed, F1174 mutations were present in 5 of 27 *MYCN*-amplified cell lines whereas only one R1275 mutation was present in this cohort (Supplementary Table S2).

Frequency of *ALK* mutations according to genomic subtype

To further explore the relationship between *ALK* mutation status and genomic alterations, we classified the tumors into genomic subclasses based on arrayCGH data (3). For 659 tumors, we could establish the genomic subtype: subtype 1 with numerical imbalances only ($n = 218$), subtype 2A with 11q deletion and without *MYCN* amplification ($n = 126$), subtype 2B with *MYCN* amplification ($n = 158$), and subtype 3 without any detectable DNA copy number alterations ($n = 78$). This classification covered most of the cases (88%), with 79 remaining unclassified (Supplementary Fig. S2).

A comparison of the *ALK* mutation frequency in relation to genomic subtype revealed that *ALK* mutations were most frequently observed in *MYCN*-amplified tumors (subtype 2B; 8.9% mutated), followed by subtype 1 tumors (7.3% mutated), subtype 2A tumors (4.0%), and subtype 3 tumors (1.3%). Interestingly, all infrequent mutations (6 of 49) were present in subtype 1 tumors (Fig. 1B).

Correlation of *ALK* mutation with survival

No significant survival differences were found in tumors with or without *ALK* mutations (or amplifications; log-rank $P = 0.317$; Fig. 2A). However, when the survival of patients with R1275 mutation or wild-type patients was compared with patients with the F1174 mutation type, Kaplan-Meier analysis showed significant survival differences ($P = 0.027$ and $P = 0.002$; Fig. 2B and C). This might largely be explained by the high frequency of *MYCN* amplification within the F1174 mutated tumors compared with the R1275 mutated tumors.

Interestingly, although not statistically significant, we noticed that 9 of 10 patients with a *MYCN* amplification and F1174 mutation died of disease, suggesting that within the *MYCN*-amplified subgroup, patients with the F1174 mutation may have a particularly poor survival as compared with a 32% 5-year overall survival rate for *MYCN*-amplified cases without the F1174 mutation.

ALK amplification

Overall, *ALK* amplifications could be detected in only 12 of 709 tumors (1.7%), and none of these carried activating *ALK* mutations. All *ALK*-amplified tumors, except for one, were also found to be *MYCN* amplified ($P < 0.001$), which accounts for 6.7% of the total of *MYCN*-amplified tumors. Like *ALK* mutation, amplification is not a statistically significant independent marker for survival